Modification of Local and Global Conformational Stability of Hemoglobin by the Allosteric Effectors BPG and IHP

Md. Eaqub Ali

A Thesis
in
The Department
of
Chemistry and Biochemistry

Presented in Partial Fulfilment of the Requirements

For the Degree of Master of Science at

Concordia University

Montreal, Quebec, Canada

May 2004

Your file Votre référence
ISBN: 0-612-94664-9
Our file Notre référence
ISBN: 0-612-94664-9

ABSTRACT

Modification of Local and Global Conformational Stability of Hemoglobin by the Allosteric Effectors BPG and IHP

Md. Eaqub Ali

FTIR studies of the effects of BPG and IHP binding on the ν(SH) stretching vibrations of human deoxyhemoglobin A (deoxyHbA) between 25 and 75°C reveal that the effectors stabilize the ν(SH) peak of Cysβ93 at 2576 cm^{-1} at high temperatures (55°C or above). In the presence of the effectors, the ν(SH) peak of Cysα104 at 2558 cm^{-1} is broadened, and the ν(SH) shoulder of Cysβ112 at 2564 cm^{-1} fluctuates in intensity with increasing temperature, indicating that the effectors destabilize the $\alpha_1\beta_1$ interface of the deoxyHbA tetramer ($2\alpha2\beta$).

At 25°C, the Soret CD bands of 0.5 mM effector-bound deoxyHbA are observed at 418 and 432 nm with ellipticities of -2.4 and +28 $M^{-1}cm^{-1}$, respectively. These signals are intensified by 2-5 units at 55°C. In contrast, effector-free deoxyHbA loses ~50% of its Soret CD absorption and ~10% of its unpolarized Soret absorption on heating to 55°C. Effector binding also stabilizes the 287-nm negative CD band and the three-valley CD absorption between 250-270-nm, which reflect changes at the $\alpha_1\beta_2$ interface.

FTIR-monitored thermal unfolding of 3.0 mM deoxyHbA reveals that loss of the α-helical absorption at 1653 cm^{-1} occurs in three phases. These may be associated with tetramer→ dimer, dimer→ monomer and monomer→ denatured-monomer transitions. In the presence of BPG and IHP, the FTIR denaturation curves are shifted by ~5°C to lower temperature, indicating that effector binding destabilizes the secondary structure of deoxyHbA.

ACKNOWLEDGEMENT

I would like to express my gratitudes to Dr. Ann M. English for her support, outstanding guidance, wisdom and honesty that she gave me through my degree and for making me a better researcher. I am also thankful to Drs. Joanne Turnbull and Marcus F. Lawrence, the members of my committee, who were always available and more than willing to provide me with help and guidance. I also acknowledge the help and suggestions of Dr. C. Skinner, the Graduate Program Director in the Department.

Special thanks to my fellow lab members, David Yeung, Farida Mohammed, Ernesto Moran, Jaffar Hasnaine, Steve Spetsieries, Georgia Kremmydiotis, Lemei Tao, Mihai Cortea, Jiang Heng, Mengwei Ye and Biao Shen, who are all great people and great scientists, and who made my time spent in the lab enjoyable. I sincerely appreciate the unlimited encouragement and sacrifice made by my wife, Juwairiah Sultana, during my studies at Concordia. I would also like to thank my mother and mother-in-law for the support and encouragement that they give me always. I thankfully remember professors Rafiqur Rahman and Apala Farhad Naved in the Department of Biochemistry and Molecular Biology, University of Dhaka, Bangladesh, for comunicating with me by e-mail, and providing advice and suggestions that always encouraged me in my work.

Finally, I acknowledge the University of Science and Technology of Chittagong (USTC), Bangladesh, for granting me leave to pursue my studies at Concordia University.

TABLE OF CONTENTS

LIST OF FIGURES

LIST OF TABLES

ABBREVIATIONS

CD	Circular Dichroism
FTIR	Fourier Transform Infrared
FSD	Fourier Self-Deconvolution
SD	Second Derivative
UV-vis	Ultraviolet Visible
pdb	Protein Data Bank
μm	Micrometer
μL	Microliter
mL	Milliliter
M	Molar
mM	Millimolar
μM	Micromolar
cm^{-1}	Wavenumber or Frequency
Hb	Hemoglobin
HbA	Human Adult Hemoglobin
deoxyHb	Deoxyhemoglobin
oxyHb	Oxyhemoglobin
metHb	Methemoglobin
HbH	Hemoglobin Hirose
HbR	Hemoglobin Rouen
HbR^{1}	Hemoglobin Rothschield

1.0 Introduction

1.1 Structure and Function of Hemoglobin

Hemoglobin (Hb) (MW = 64,500) is a tetrameric protein composed of two α-chains and two β-chains. Each α-chain and each β-chains contains 141 and 146 amino acid residues, respectively. Moreover, each α-chain and each β-chain is composed of seven and eight helical segments, respectively, interrupted by turns and loops. Starting from the N-terminus, the helical segments are denoted A to H, and the nonhelical ones NA, AB, BC, etc., to HC, which is a segment of three nonhelical residues at the C-terminus. Residues within each segment are numbered from the amino end, A1 to A16, etc. The α-chains lack a D helix. The helical and nonhelical segments in each chain are listed in Table 1.1 and shown in Figure 1.1.

Each chain also carries a heme group (1,2). The hemes are held between the E and F helices in pockets formed by several helical and nonhelical segments. Each heme Fe is coordinated to N_{ε} of histidines F8 (Hisβ92 and Hisα87, respectively), also known as the proximal ligands, and to the four porphyrin nitrogens (N_{porph}). The porphyrin is in van der Waals contact with histidine E7 (Hisβ63 and Hisα58, respectively) on the distal side. It also makes contact with the side chains of another 18 amino acid residues most of which are nonpolar. The propionate side chains of the porphyrin protrude into the solvent and form hydrogen bonds with basic side chains of the globin (1,2).

In tetrameric Hb the α and β subunits are symmetrically arranged by noncovalent interactions around a central water-filled cavity (1-6). The αβ interactions are stronger

Table 1.1: Helical and nonhelical segments in α- and β-chains of HbA

Segment[a]	α-chain position[b]	β-chain position[b]
NA	Val1-Leu2	Val1-His2
A	Ser3-Gly18	Leu3-Val18
AB	Ala19	Asn19
B	His20-Leu34	Val20-Tyr34)
C	Ser35-Tyr42	Pro35-Phe41
CD	Phe43-Gly51	Phe42-Ser49
D	Absent	Thr50-Gly56
E	Ser52-His72	Asn57-His77
EF	Val73-Leu78	Leu78-Thr84
F	Leu79-Ala88	Phe85-Cys93
FG	His89-Val93	Asp94-Val98
G	Asp94-His112	Asp99-His117
H	Thr118-Ser38	Thr123-His143
HC	Lys139-Arg141	Lys144-His146

[a] Helical segments are denoted A, B, ...H and the nonhelical segments are denoted NA, AB,.....HC.

[b] The proximal histidines (F8) are Hisα87 and Hisβ92 in the α- and β-chains, respectively. The corresponding distal histidines (E7) are Hisα58 and Hisβ63.

than the αα or ββ interactions. Consequently, tetrameric Hb dissociates into αβ dimers rather than into αα or ββ dimers in solution. Upon binding of molecular oxygen (O_2), the protein undergoes structural changes whereby the $\alpha_1\beta_1$ and $\alpha_2\beta_2$ dimers are shifted at the dimer interface (1, 2). The two structures, termed T for tense or deoxy or low affinity, and R for relaxed or oxy or high affinity, differ in the arrangement of the four subunits,

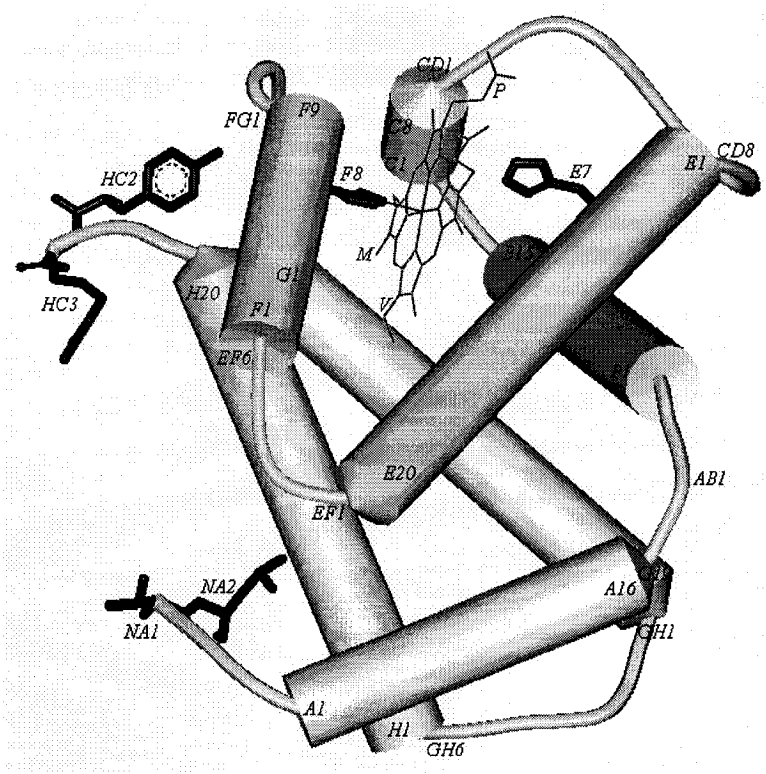

Fig 1.1: Secondary and tertiary structures of Hb α-chains showing the α-carbons and the coordination of the heme. Starting from the N-terminus the helical segments are denoted A to H, and the connecting loops NA, AB, BC, ...HC. Shown are the side chains of the proximal histidine F8 (Hisα87) linked to the heme iron, the distal histidine E7 (Hisα58), valine E11 (Valα62), and the two N-terminal (Valα1and Leuα2) and the two C-terminal (Tyrα140 and Argα141) residues denoted by NA1, NA2, and HC2, HC3, respectively, all of which are important in ligand binding. The protoporphyrin IX is in solid lines and M, V and P stand for its methyl, vinyl and proprionate side chains, respectively. This diagram was generated by using PDB file 1k1k and Web Labviewerlite. The numbering is that of Perutz *et al.* (2).

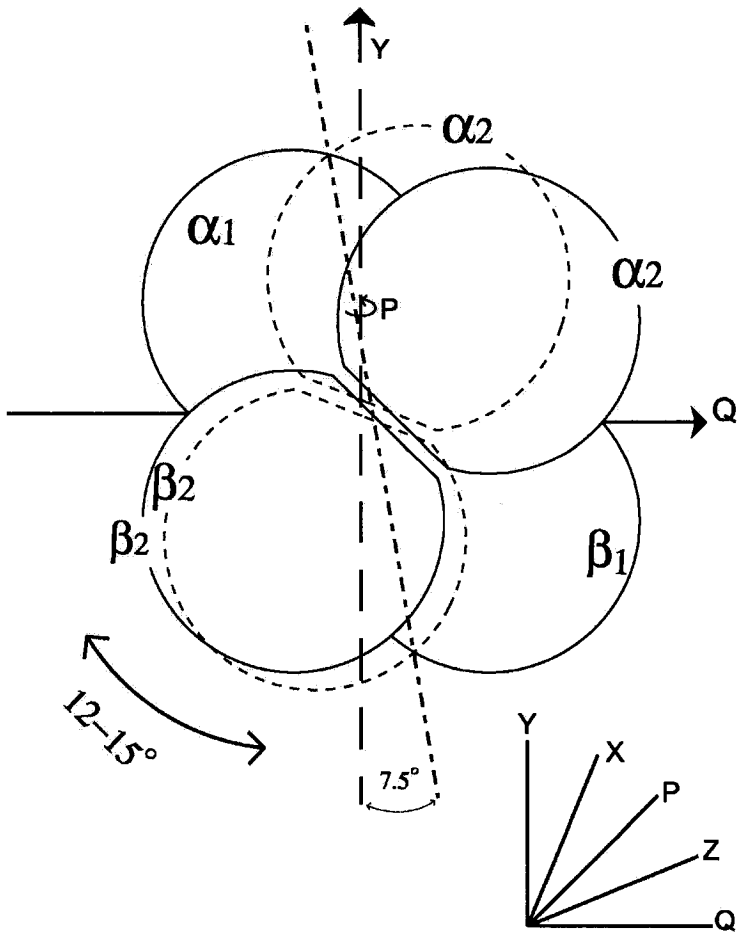

Fig 1.2: Schematic diagram illustrating the change in quaternary structure that accompanies ligation of Hb. In the diagram, the liganded (broken lines) and unliganded (solid lines) $\alpha_1\beta_1$ dimers are superimposed. The position of the liganded $\alpha_2\beta_2$ dimer corresponds to that obtained by rotating the unliganded $\alpha_2\beta_2$ dimer about an axis P by an angle θ = 12-15° and shifting it along axis P by 1 Å into the page (this axis is perpendicular to the dyad symmetry axes, marked Y, of both the liganded and unliganded Hb molecules and to the plane of the page). Note that ligation causes little movement of the α_1 and β_1 or the α_2 and β_2 subunits relative to each other. The diagram was adapted from that given by Perutz *et al.* (1).

(referred to as the quaternary structure) and in the conformation of the subunits (referred to as the tertiary structure). The quaternary R $\leftrightarrow$ T transition consists of rotation of the $\alpha_1\beta_1$ dimer relative to the dimer $\alpha_2\beta_2$ by 12-15°, and translation of one dimer relative to the other by 0.8 Å (Figure 1.2). The two β subunits are about 5 Å further apart in the quaternary T structure than in the R structure.

The ferrous heme Fe is five-coordinate, high spin and about 0.5 Å displaced from the plane of the porphyrin. It is constrained by salt bridges (Table 1.2) between the C-termini of the four subunits. In the quaternary R structure, these salt bridges are broken and the ferrous heme Fe is six-coordinate, low spin and in the plane of the porphyrin (1-6). AquometHb exists in the R structure but displays intermediate character of oxy- and deoxy-forms. The ferric heme Fe in aquometHb is six-coordinate, where the sixth position is occupied by a H_2O molecule. This water molecule is replaceable by several ligands such as fluoride, azide, cyanide and hydroxyl but not by molecular oxygen (4). The radius of the ferric ion varies with its spin state from 0.55 Å in low spin to 0.60 Å in high spin ferric compounds. The ferric ion is small enough to fit into the plane of the porphyrin. CyanometHb is purely low spin and fluorometHb is purely high spin. However, the heme iron in aquometHb is 0.3 Å displaced from the plane of the porphyrin (4). Addition of equimolar inositol hexaphosphate (IHP) to a solution of aquometHb forces it to assume T structure (3, 4).

Hemoglobin's main function is the transport of O_2 from the lungs to the tissues and CO_2 from the tissues to the lungs (1,2). The oxygen affinity of mammalian Hbs is lowered by H^+, Cl^-, CO_2 and 2,3-bisphosphoglycerate (BPG), all of which are present in red blood cells. They are collectively known as allosteric effectors. Hb binds one H^+ for

every two O_2 molecules released. This drives the equilibrium of the reaction between CO_2 and H_2O in the direction of the product HCO_3^-, promoting the transport of CO_2 by the blood stream (1,2):

$$CO_2 + H_2O \rightleftharpoons HCO_3^- + H^+ \quad (1)$$

Protons released by the metabolic products, lactic and carbonic acids, facilitate the release of O_2 to the tissues (1).

Although Hb is predominantly involved in O_2 and CO_2 transport in vertebrates, recently it has been implicated in nitric oxide (NO) transport and delivery. Hb in the R state binds NO at Cysβ93, forming Hb-SNO that acts as a hormone and delivers NO to tissues and thereby causing vasodilatation and increased blood flow. Thus, Hb may function as a blood pressure regulator in an oxygen-sensitive manner (7).

In 1970, the atomic structures of oxy- and deoxyHb were determined. Since then Hb has been used as a model of allostery in biological systems (1). It is also an ideal molecule to study heme coordination complexes that are formed in a variety of catalytic and other actions in biological systems. In short, understanding the functions of Hb is fundamental to understanding the functions of proteins in general. Considering all of these factors, Hopfield called Hb "the hydrogen atom" of biochemistry (2).

1.2 The Theory of Allostery

In 1965, Monod, Weyman and Changeux published their theory of allostery, now commonly known as MWC theory (9-10). When Monod conceived the idea that allosteric proteins control and coordinate chemical events in the living cells, he said that he had discovered the second secret of life. The first secret was the structure of DNA (10). According to MWC theory, cooperative substrate binding and modification of

enzymatic activity by metabolites bearing no stereochemical relationship to either substrate or product may arise in proteins with two or more structures in equilibrium. It predicts that such proteins are composed of several symmetrically arranged subunits with structures that differ by the arrangement of the subunits and number and/or strength of the bonds between them. In one structure the subunits would be constrained by strong bonds that would resist the tertiary changes needed for substrate binding. They called this structure "T" for tense. In the other structure these constraints would be broken or relaxed and they called it "R" for relaxed. Between R↔T transitions, the symmetry of the molecule must be conserved, so that the activity of the subunits would be either equally low or equally high (1, 12). In 1966 Koshland *et al.* published their sequential model to explain the allosteric events in multimeric proteins (11). The highlight of this model was that it did not invoke any restrictions allowing each subunit to change its tertiary structure upon substrate binding and thereby to affect the chemical activities of its neighbors. The biological advantage of allosteric enzymes is that no direct interaction need occur between the substrate or product of the protein and the regulatory metabolite that controls its activity because control is entirely due to a change of structure induced in the protein when it binds its specific effectors (1).

The α and β subunits of Hb are symmetrically disposed around a central water-filled cavity. The four hemes in the four subunits are surface exposed and separated from each other. In the R structure the Fe-Fe separation between the α-chains is 36 Å and 33 Å between the β-chains. In the T structure, the corresponding distances are 35 Å and 40 Å. The cooperativity or heme-heme interaction in Hb is defined as the rise of oxygen affinity of a Hb solution with rising oxygen saturation. Cooperativity is possible because of the

quaternary and tertiary structural changes of the globin chains as well as the spin state and position of the heme iron relative to the porphyrin and the globin (1-7). As discussed above (Section 1.1), the transition between the T and R structures consists of a rotation and translation of one $\alpha\beta$ dimer relative to the other. The $\alpha\beta$ dimers move relative to each other at the symmetry-related contacts $\alpha_1\beta_2$ and $\alpha_2\beta_1$, and at the contacts $\alpha_1\alpha_2$ and $\beta_1\beta_2$ (Figure 1.2). The contacts $\alpha_1\beta_1$ and $\alpha_2\beta_2$ remain rigid. The additional bonds, predicted by MWC, were found to consist of C-terminal salt-bridges between and within the subunits in the T structures (Table 1.2). At the $\alpha_1\beta_2$ interface, the nonhelical segment $FG\alpha_1$ is in contact with helix $C\beta_2$, and helix $C\alpha_1$ with $FG\beta_2$. During the R$\rightarrow$ T transition, the contact $FG\alpha_1$ — $C\beta_2$ acts as a ball and socket joint, while the contact $C\alpha_1$— $FG\beta_2$ acts as a two-way switch that shifts $C\alpha_1$ relative to $FG\beta_2$ by about 6 Å, like the knuckles of one hand moving over those of the other.

The intermediate positions of the switch are blocked by steric hindrance imposed by the distal histidine (E7) and the distal valine (E11). The gaps along the central cavity between α_1 and α_2, and between β_1 and β_2 narrow on the T$\rightarrow$R transition. The shape of the $\alpha_1\beta_1$ and $\alpha_2\beta_2$ dimer is altered by changes in tertiary structure. For example, on oxygenation the distance between the α-carbons of residues $FG1\alpha_1$ and $FG\beta_1$ shrinks from 45.6 to 41.3 Å. These changes make an $\alpha_1\beta_1$ dimer with a tertiary oxy structure a misfit in the quaternary T structure, and an $\alpha_1\beta_1$ dimer with a tertiary deoxy structure a misfit in the quaternary R structure (1, 2, 12).

The regulator 2,3-bisphosphoglycerate (BPG) binds to a stereochemically complimentary site in the central cavity between the β-chains in the T structure and biases the equilibrium towards T. During the T$\rightarrow$R transition this complementarity is

Table1.2: Salt bridges (...) and hydrogen bonds (---) within and between the subunits that stabilize the T or R structure of HbA

T structure		
Interaction within subunits	Interactions between subuints	Loss of interactions sufficieint to tip unliganded Hb fully to the R structure
(1) Tyrα140-OH--- OC-Valα93	(6) Lys$\alpha_1$127-NH_3^+...$^-$OOC-Arg$\alpha_2$141	
(2) Tyrβ145-OH --- OC-Valβ98	(7) Asp$\alpha_1$126-COO^-...$^+$Gua-Arg$\alpha_2$141	Interactions (1), (6) and (7) are lost in Des-Argα141-Tyrα140[c]
(3) Hisβ146-Im^+..$^-$OOCAspβ94	(8) Lys$\alpha_1$40-NH_3^+ ... $^-$OOC-His$\beta_2$146	Interactions (2), (4) and (5) are lost in Hb Bethesda (Tyrβ145$\rightarrow$ His)[f]
(4) PO_4^{2-} ... $^+NH_3$-Valβ1	(9) Valβ1-NH_3^+ ... BPG[a]	
(5) PO_4^{2-} ... $^+NH_3$-Lysβ82	(10) Lysβ82 -NH_3^+ --- BPG[a]	Interactions (3), (6), (7) and (8) are disrupted in Nes-des-Argα141[e] and Des-Argα141-Hisβ146[d]
	(11) Hisβ2-Im^+ --- BPG[a]	
	(12) Hisβ143-Im^+ --- BPG[a]	Interaction (13) is lost in Hb Kempsey (Aspβ99$\rightarrow$Asn)[f]
	(13) Tyr$\alpha_1$42-OH --- OOC-Asp$\beta_2$99	
R structure		
	(14) Lys$\alpha_1$127-NH_3^+...$^-$OOC-Arg$\alpha_2$141[b]	Loss of interactions sufficieint to tip liganded Hb fully to the T-structure
	(15) Valβ1-NH_3^+ ... $^-$OOC-His$\beta_2$146[b]	
	(16) Asp$\alpha_1$94-COO- --- NH_2-Asn$\beta_2$102	Interaction (16) is lost in Hb Kansas (Asnβ102$\rightarrow$ Thr)[f]

[a] BPG, 2,3-bisphosphoglycerate; [b] probably a very weak salt bridge; [c] Des-Argα141-Tyrα140, HbA minus C-terminal Argα141 and Tyrα140; [d] Des-Argα141-Hisβ146, HbA minus Argα141 and Hisβ146; [e] Nes-des-Argα141, HbA minus Argα141 and N-ehthylmeleimide (NEM) modified Cysβ93; [f] Hb Bethesda, Hb Kansas and Hb Kemsey are naturally occurring variants of HbA (3).

disrupted due to the breaking of the C-terminal salt bridges that constrain the T structure and to the narrowing of the central cavity between the β-chains (13-15).

1.3 Heme Stereochemistry in Oxy- and DeoxyHb

An allosteric core, composed of the heme, histidine F8, the FG corner and the part of the F-helix, plays an essential role in ligand-induced structural changes in Hb (12). In deoxyHb, the porphyrins are domed and the Fe(II) ions are displaced from the planes of

the porphyrins by 0.5-0.6 Å. Oxygenation flattens the porphyrins and the Fe-N_{porph} bonds contract which causes the metal to move into the plane of the porphyrin (Figure 1.3). A water molecule that is hydrogen bonded to the distal Hisα58 (E7) in deoxyHb dissociates in oxyHb (1,2,12). The degree of doming of the porphyrins appears to be influenced by the constraints of the globin. The movement of the metal is transmitted to the proximal Hisα87 and Hisβ92 (F8) and their adjoining residues are perturbed, while the bulk of the protein remains unperturbed. The side chains of Leuα91 and Leuβ96 (FG3), and Valα93 and Valβ98 (FG5) are pushed down. This perturbation is transmitted to the $\alpha_1\beta_2$ and $\alpha_2\beta_1$ contacts and the residues at these interfaces experience a major shift and environmental changes.

Replacement of hydrogen-bonded H_2O by O_2 in the distal pockets of the α subunits does not cause perceptible perturbation of the distal residues. However, in the β subunits, the displacement of the distal Hisβ63 (E7) and distal Valβ67 (E11) is essential for the binding of O_2 to the ferrous hemes. Since C_α-C_β bond rotation is restricted in valine residues in an α-helix, Valβ67 cannot move relative to the heme without displacement of helix E. Crystals of deoxyHbA grown in PEG (polyethyleneglycol) and exposed to air show full saturation with oxygen at the α-hemes but no binding at the β-hemes. This reveals that the β-hemes have little or no O_2 affinity in the crystalline T structure. However, in solution, the β-hemes display only 1.5- to 3-fold less O_2 affinity than that of the α-hemes and 4-times faster reaction with O_2 than the α-hemes. This is due to a transition in solution in the tertiary structure of the β-subunits that displaces Valβ67 residues from the distal pockets. This transition is inhibited by lattice constraints in deoxyHb crystals (1, 2,13). It has been confirmed by site-directed mutagenesis studies

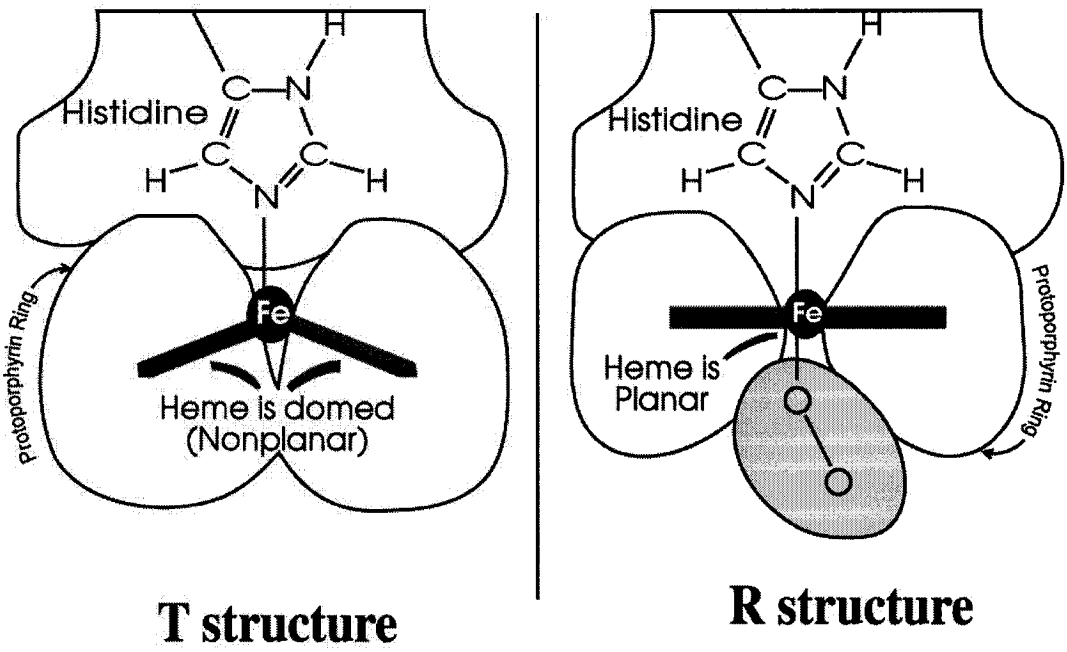

Fig 1.3: Heme stereochemistry in the T and R structures of HbA. In the T structure, the porphyrin ring is domed and the Fe(II) ion is displaced from the plane of the porphyrin. In the R structure, the porphyrin ring is flattened and the Fe(II) is in the porphyrin plane (2).

that steric hindrance to ligand binding to the β-hemes in the T structure comes from Valβ67 and not from the distal Hisβ63(7).

1.4 Binding of BPG to Hb

2,3-Bisphosphoglycerate (BPG) is a dominant allosteric effector for mammalian Hbs, particularly for adult human Hb (HbA). On BPG binding, the affinity of Hb for O_2 is reduced and hence the release of O_2 to the tissues is greatly favoured. This function of BPG becomes extremely important in high altitudes where pO_2 is low and also under certain pathological conditions such as anemia. BPG binds to a complementary site in Hb called the BPG binding domain (13-15), which is located in HbA at the entrance to the central cavity between the N-termini of the β-chains. BPG is surrounded by four pairs of basic groups, the N-terminal amino groups (Valβ1), Hisβ2, Hisβ143 and Lysβ82 (13-15). This site is only formed in deoxyHb although BPG also binds oxyHb and metHb (3). It supposedly binds to the same site in metHb and oxyHb but the binding sites in metHb and oxyHb have not been characterized (3,13-15).

In deoxyHbA, a charged $NH_3^+ - {}^-OOC$ hydrogen bond is formed between the ε-amino group of Lysβ82 and the carboxylate group of BPG (Table 1.1, Figures 1.4 and 1.5). Complete deprotonation of the phosphate groups of BPG triggers strong electrostatic stress within the Hb molecule, which is manifestated by changes in tertiary and quaternary structure (1-4,13-15). The N-terminal amino groups (Valβ1) interact with BPG *via* salt bridges or electrostatic interactions between NH_3^+ and the negatively charged phosphate groups. The side chains of Hisβ2 and Hisβ143 form hydrogen bonds with the phosphate groups. These five hydrogen bonds (Figure 1.4) and two salt bridges involving Valβ1 allow BPG to trigger a conformational change in Hb that favours the T

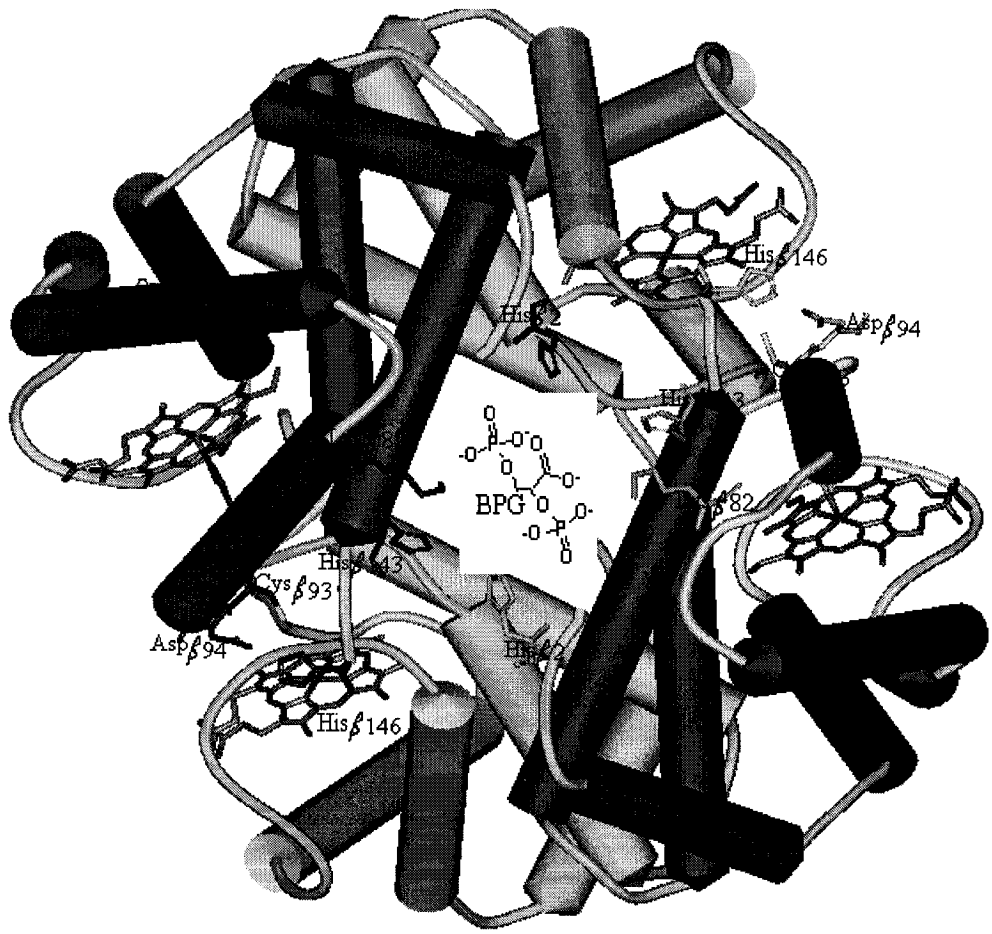

Fig 1.4: Crystal structure of deoxyHbA showing the BPG binding site. The white and the black cylinders represent the α-helices of α-chains and β-chains, respectively, and the white connectors represent β-turns. The figure also shows the imidazole group of Hisβ146 and the carboxylate group of Aspβ94, which form salt bridges that screen the SH group of Cysβ93 in the T structure. This figure was generated by WebLabviewerlite using the PDB file 1gzx.

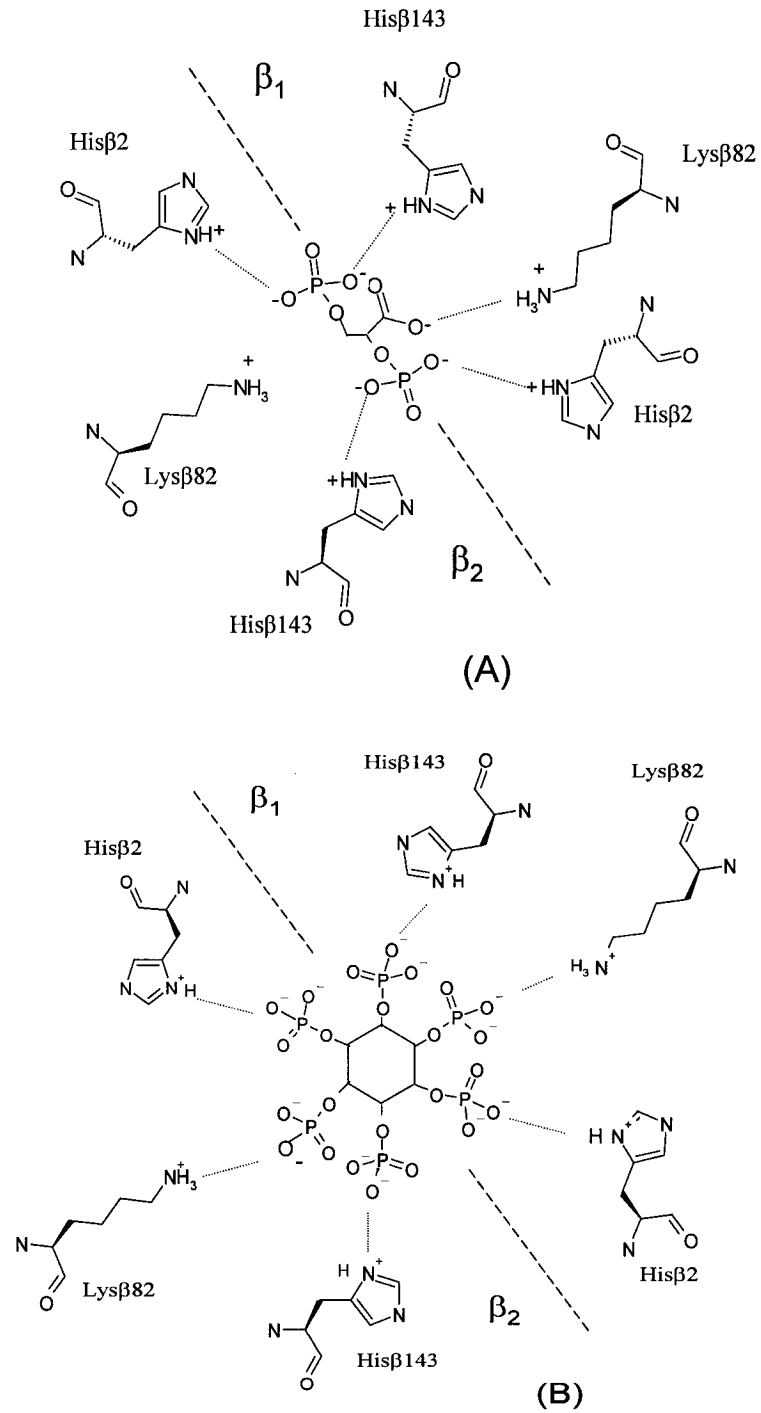

Fig 1.5: Interactions of BPG (A) and IHP (B) with deoxyHbA. Note that BPG forms five H-bonds and IHP forms 6 H-bonds. The salt bridges between Valβ1 and BPG or IHP (Table 1.2) are not shown in this figure, which was generated by ISIS draw 2.4 (13,14).

structure over the R structure and hence the affinity for O_2 is reduced.

Several other multivalent anions, such as inositol hexaphosphate (IHP), ATP, GTP and $[Fe(CN)_6]^{4-}$ also lower the oxygen affinity of HbA (14). The most effective is IHP, which bears structural homology to inositol pentaphosphate (IPP) that regulates the O_2 affinity of avian erythrocytes (10). IHP binds to the same sites as BPG in human deoxyHbA and the six phosphate groups of IHP interact with the same residues, Valβ1, Hisβ2, Hisβ143 and Lysβ82 in the BPG binding domain. However, binding of IHP is stronger than BPG and produces more pronounced structural changes in human HbA because it makes one additional hydrogen bond with Lysβ82 (Figure 1.5) (13, 15). The carboxyl group of BPG forms hydrogen bonds with only one of the two Lysβ82 residues while IHP forms hydrogen bonds with both. Hence, the total number of hydrogen bonds formed by BPG and IHP is five and six, respectively. IPP occupies the same position in chicken Hb as IHP does in HbA. However, 12 basic groups interact with IPP in chicken Hb *vs* eight in HbA, and include Valβ1, Hisβ2, Lysβ82, Argβ135, Hisβ139 and Argβ143 (14) from each β-subunit of chicken Hb.

1.5 Hypothesis, Scope and Organization of Thesis

The allosteric transition of Hb, the switching of T to R structure on oxygenation, is accompanied by changes in quaternary and tertiary structures of the molecule as well as by a change in the spin state and position of the heme iron relative to the porphyrin and globin (1-6). As discussed in Section 1.4, the allosteric effectors BPG and IHP cross-link the two β-chains of Hb, forming H-bonds and salt bridges with Hisβ2, Lysβ82, Hisβ143 and Valβ1, and favour the T structure. It is hypothesized here that this cross-linking of the β chains by the effectors stabilizes the $\alpha_1\beta_2$ and $\alpha_2\beta_1$ interfaces and destabilizes the

$\alpha_1\beta_1$ and $\alpha_2\beta_2$ interfaces. These effector-induced changes in the local or global conformational stability of deoxyHbA can be probed spectroscopically by altering the temperature.

Cysβ93 of HbA is located at the $\alpha_1\beta_2$ interface and is the focus of intense interest due to its proposed role in NO-binding and delivery in an oxygen-sensitive manner (7). It has been observed that HbA mutated or chemically modified at Cysβ93 shows higher oxygen affinity, reduced cooperativity, lower Bohr effect and reduced response to the allosteric effectors BPG and IHP that stabilize the T structure of Hb (8). Since the observations made with altered or modified Cysβ93 are important for allosteric switching of HbA, a detailed study of the effects of BPG and IHP on the environmental stability of Cysβ93 in deoxyHbA is presented in Chapter 2. The effect of the allosteric effectors on Cysα104 and Cysβ112, which are located in a relatively inert surface, are also studied in this chapter. In Chapter 3, the effects of BPG and IHP on the environmental stability of the heme, the site of initiation of the allosteric transition on ligand binding, are probed in deoxyHbA by circular dichroism (CD) and unpolarized ultraviolet-visible (UV-vis) spectroscopy. The environmental changes around the aromatic residues in the T and R structures are also investigated by CD. Changes in secondary structure are reported in Chapter 4. FTIR spectroscopy and far-UV CD were used to monitor the thermal stability of the secondary structure of deoxyHbA on BPG and IHP binding. Conclusions and suggestions for future work are presented in Chapter 5.

2.0 Effects of BPG and IHP on the Environment of the Cysteine Residues in DeoxyHbA

2.1 Abstract

The effects of 2,3-bisphophoglycerate (BPG) and inositol hexaphosphate (IHP) on the sulfhydryl groups of adult human deoxyhemoglobin (deoxyHbA) were studied by Fourier transform infrared (FTIR) spectroscopy between 25 and 75°C with a temperature interval of 5°. A relatively intense ν(SH) peak at 2576 cm^{-1} at high temperature in the presence of BPG and IHP reveals that effector binding stabilizes the polar environment of Cysβ93 at the $\alpha_1\beta_2$ interface in deoxyHbA. Broadening of the Cysα104 peak at 2558 cm^{-1} at high temperature with IHP present reveals destabilization of the $\alpha_1\beta_1$ interface. The fluctuating frequencies and intensities of the Cysβ112 shoulder at different temperatures in the presence of the effectors confirm that these ligands disturb the environment of residues at the $\alpha_1\beta_1$ interface. The thermal stability of free BPG in water was also evaluated by FTIR. The three BPG peaks assigned to ν(P-OC), ν(CH-OP) and ν(CH_2-OP) of BPG were observed at 1055, 1089 and 1119 cm^{-1} between 25 and 75°C indicating that BPG was stable under the experimental conditions employed.

2.2 Introduction

The allosteric effectors BPG and IHP bind to the central cavity formed by the two β-chains of Hb forming hydrogen bonds and salt bridges with positively charged residues (Figure 1.5). The phosphate groups of BPG and IHP are deprotonated at physiological pH causing a strong electrostatic stress within the Hb molecule. The hydrogen bonds and salt bridges formed by BPG and IHP with the β-chain residues force the Hb molecule into the

deoxy or tense (T) conformation. As a result, the T structure is favoured over the R structure, which allows Hb to liberate O_2 to the tissues under low oxygen pressure such as found at high altitudes (13-14). Adult human hemoglobin (HbA) has six cysteine residues, none of which are involved in disulfide bonding. Cysα104 and Cysβ112 are burried at the $\alpha_1\beta_1$ and $\alpha_2\beta_2$ subunit interfaces, which are relatively resistant to change on the T→R transition (19). DeoxyHb possesses 32 and oxyHb 34 amino acid residues at the $\alpha_1\beta_1$ contact, respectively. FTIR-monitored ν(SH) absorption of Cysα104 and Cysβ112 revealed changes in the $\alpha_1\beta_1$ and $\alpha_2\beta_2$ subunit interfaces on the T→ R transition, which were not detected by other approaches (19).

Cysβ93 is located adjacent to the proximal Hisβ92 at the $\alpha_1\beta_2$ interface, a site that undergoes changes on T→ R transition. Since the allosteric changes that originate at the heme upon ligand binding are believed to dissipate into the globin through the proximal Hisα87 and Hisβ92 (F8) (1-6), Cysβ93 is strategically situated to study the T→ R transition. The crystal structure shows that the thiol group of Cysβ93 protrudes into a hydrophobic environment in oxyHbA but is surface exposed and shielded by a salt bridge between Hisβ146 and Aspβ94 in deoxyHbA (Figure 1.4). Cysβ93 is also very close to the BPG binding domain that includes Valβ1, Hisβ2, Lysβ82 and Hisβ143 (Figure 1.4). BPG binds to its pocket forming five hydrogen bonds and two salt bridges (13-15, Figure 1.5). The energy released by the formation of these bonds probably triggers the R→ T transition. Recombinant and chemically modified Hbs altered at Cysβ93 show higher oxygen affinity, reduced cooperativity, reduced Bohr effect and little response to BPG and IHP. Modification of Cysβ93 results in changes in the environment of several histidine residues (8) including Hisβ146 that forms a salt bridge with Aspβ94 (Figure

1.4) and screens the thiol group of Cysβ93 in deoxyHbA. Cysβ93 is not S-nitrosated by CysSNO or GSNO in deoxyHbA (7). The effects of pH on the ν(SH) vibrations of deoxy- and carbonmonoxyHbA suggest that H-bonding contributes to the environmental stability of the different cysteine residues (22). Here the thermal stability of the environment of the cysteine residues upon BPG and IHP binding to deoxyHbA are investigated by FTIR spectroscopy. The purpose of the present investigations is to characterize the environment of the different cysteines of HbA under deoxy conditions in the presence of the allosteric effectors.

2.3 Experimental Procedures

2.3.1 Materials

Human hemoglobin A, BPG (tri-sodium salt) and IHP (sodium salt) were purchased from Sigma-Aldrich and were used without further purification. Purified sodium dithionite was obtained from Fisher and the sodium salts of phosphoric acid were from Anachemica. NAP10 Sephadex G-25 columns (DNA grade) were purchased from Amersham Pharmacia Biotech. Nanopure water (specific resistance 18 MΩ-cm), obtained from a Milllipore Simplicity water purification system, was used to prepare all buffers and H_2O solutions.

2.3.2 Methods

Typically 1.0 g of lyophilized metHbA from the bottle was dissolved in 0.2 M sodium phosphate (NaPi) buffer (pH 6.5), centrifuged at 11,750g for 2 min and the supernatant was stored at 4°C prior to use. DeoxyHbA was prepared inside a glove box (MBraun-Unilab) by reacting 7 mM metHbA with 2x molar excess of sodium dithionite in the same buffer, and HbA was desalted on a NAP10 column equilibrated with the same

buffer. The concentrations of all forms of Hb were determined spectrophotometrically (ε_{500} =10 and ε_{630} = 4.4 mM^{-1} cm^{-1} $heme^{-1}$ for metHbA, ε_{555} =12.5 mM^{-1} cm^{-1} $heme^{-1}$ for deoxyHbA, and ε_{541} =13.5 and ε_{576}=14.6 mM^{-1} cm^{-1} $heme^{-1}$ for oxyHbA) in an FTIR cell with a 6-μm pathlength (teflon spacer) using a custom-made bracket in Beckman DU 650 UV-vis spectrometer. BPG (MW = 266.0) and IHP (MW = 660.0) solutions were prepared by weight in the same buffer. A 5 μL-aliquot of 100 mM BPG or IHP was added to 100 μL of 5.0 mM (tetramer) deoxyHbA and 30 μL of this solution was loaded inside the glove box onto one window of an FTIR cell, which consisted of a temperature-controlled cell mount (Harrick) and two 13 × 2 mm CaF_2 windows separated by 250-μm spacer. A control sample was prepared by adding 5 μL of buffer to 100 μL of 5.0 mM deoxyHbA. The spectra were recorded from 25 to 75°C with a temperature interval of 5° on a Nicolet Magna IR 550 Series II FTIR spectrometer equipped with an MCT detector and purged with dry air from a Whatman FTIR Purge Gas Generator (Model 75-52). At each temperature, the cell was equilibrated for 5 min and each spectrum was an average of 512 scans with a resolution of 2 cm^{-1} and an aperture of 32. The IR cell temperature was controlled using an Omega CN8500 temperature controller and monitored with a thermocouple placed in close proximity to the CaF_2 windows. Approximately 15 min before recording the spectra, the MCT detector was cooled to 77K with liquid nitrogen (Praxair). Omnic (Nicolet) software was used to perform subtraction of the buffer contribution, Fourier self deconvolution (FSD) and base line correction. To study the thermal stability of the free BPG ligand, 20 μL of 5.0 mM BPG in water was loaded into the FTIR cell with CaF_2 windows separated by a 50-μm teflon spacer (Harrick) and the spectra were collected as described above.

2.4 Results

The thiol stretching vibration, ν(SH), falls in a spectral window (2500-2600 cm^{-1}) where the transmittance of H_2O and proteins is maximum (7,19-24). The FTIR spectrum of deoxyHbA at physiological concentration (5.0 mM tetramer) recorded in the absence of BPG and IHP at 25°C exhibits three ν(SH) peaks at 2576, 2564 and 2557 cm^{-1} (Figure 3.1), which closely match the previously assigned values (Table 2.1) for Cysβ93, Cysβ112 and Cysα104, respectively (7,20,21). With equimolar BPG, deoxyHbA exhibits 1-cm^{-1} blue-shifted shoulder at 2565 cm^{-1} corresponding to Cysβ112 absorption. The Cysβ93 peak was slightly intensified while the Cysα104 peak is clearly broadened with this ligand (Figure 2.1).

Table 2.1: ν(SH) absorptions (cm^{-1}) of cysteine residues of deoxyHbA at 25 and 55°C[a]

Sample	Temperature (°C)	Cysβ93	Cysα104	Cysβ112
deoxyHbA[b]	20	2576	2557	2563
deoxyHbA[c]	25	2576±1	2557±1	2564±1
deoxyHbA[c]	55	2578±1	2557±1	2564±1
deoxyHbA + BPG[c]	25	2576±1	2557±1	2565±1
DeoxyHbA + BPG[c]	55	2578±1	2558±1	2566±1
deoxyHbA + IHP[c]	25	2576±1	2557±2	2565±1
deoxyHbA + IHP[c]	55	2578±1	2562±2	2567±1

[a] Experimental conditions are given in the legend of Figure 2.1, [b] frequencies are from (7, 20, 21) and [c] observed values are from Figure 2.1.

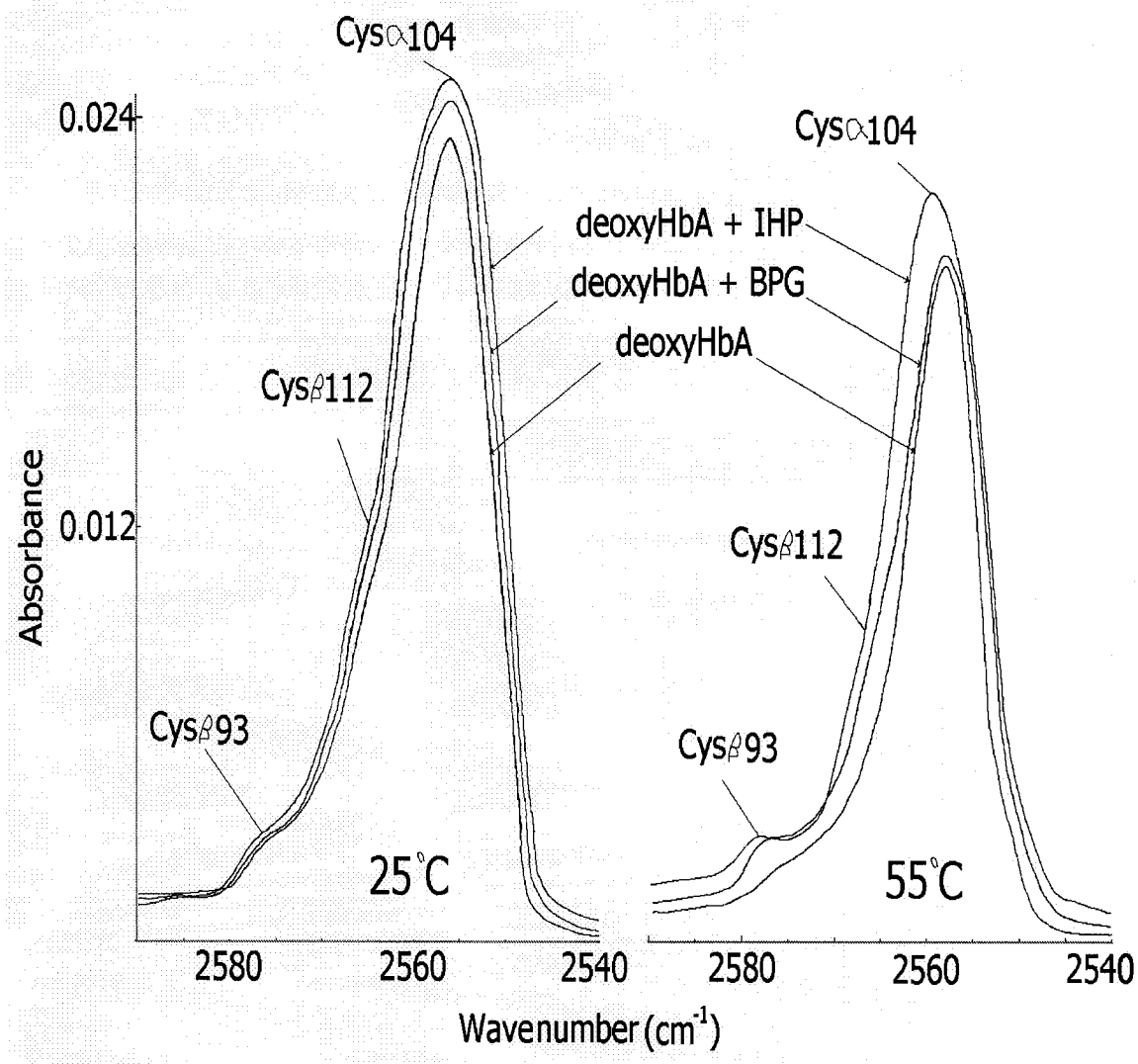

Fig 2.1: Effects of BPG and IHP binding on ν(SH) absorbtion of 5.0 mM deoxyHbA in 0.2 mM NaPi buffer (pH 6.5) at 25 and 55°C. The spectra from top to bottom are: deoxyHbA plus equimolar IHP, deoxyHbA plus equimolar BPG and deoxyHbA alone. The spectra were recorded in a temperature-controlled FTIR cell with 250-μm pathlength and a MCT detector. At each temperature the cell was equilibrated for 5 min and each spectrum is an average of 512 scans with a resolution of 2 cm^{-1}. Background subtraction, baseline correction and Fourier self-deconvolution were performed on the displayed spectra.

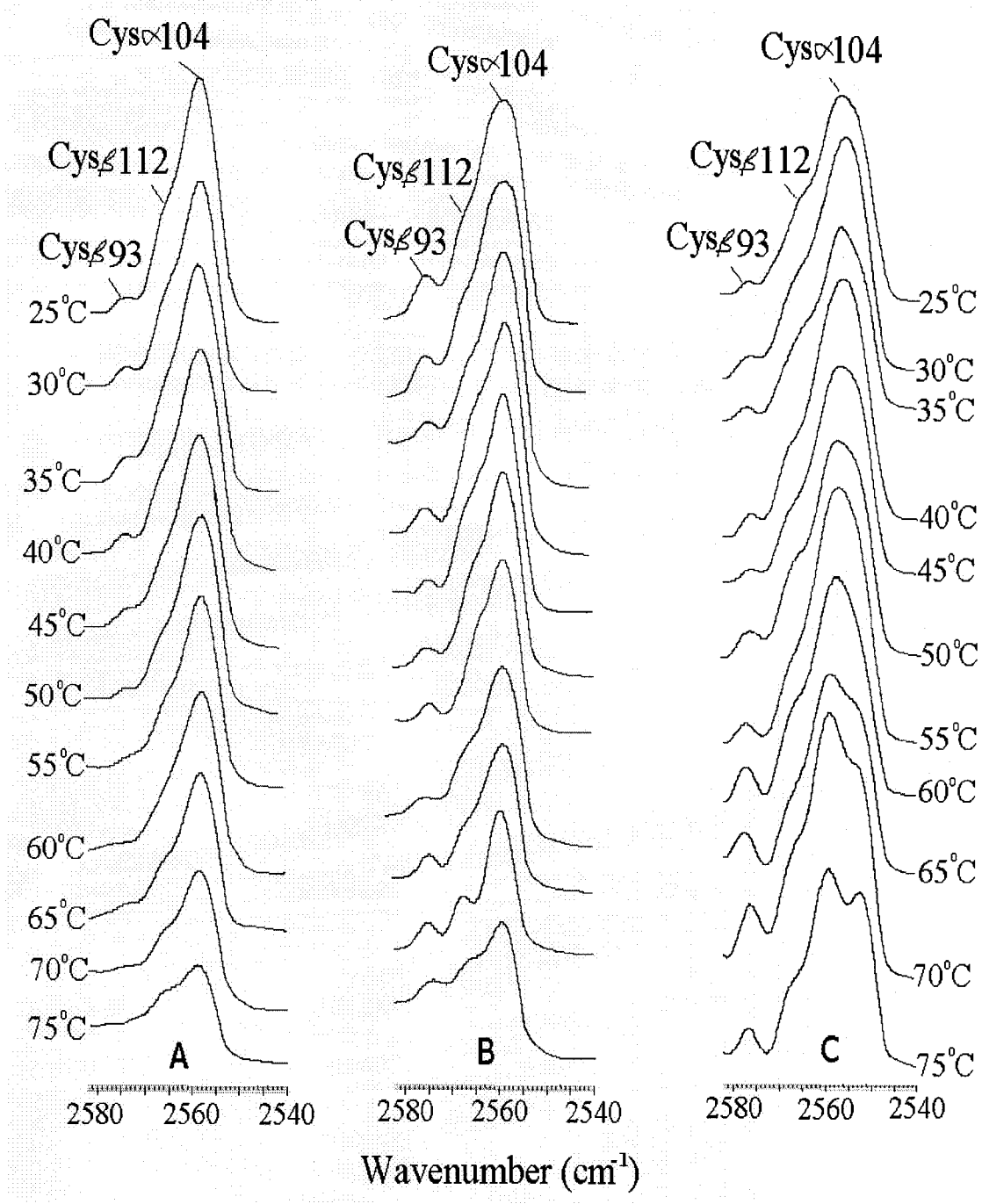

Fig 2.2: Effects of temperature and effectors on the FTIR spectra in the ν(SH) region of 5.0 mM deoxyHbA (20 mM heme) in 0.2 M NaPi buffer (pH 6.5). (A) deoxyHbA; (B) deoxyHbA with equimolar 2,3-BPG and (C) deoxyHbA with equimolar IHP. The spectra were recorded in 250-μm pathlength FTIR cell between 25 and 75°C. The experimental conditions are given in the legend of Figure 2.1.

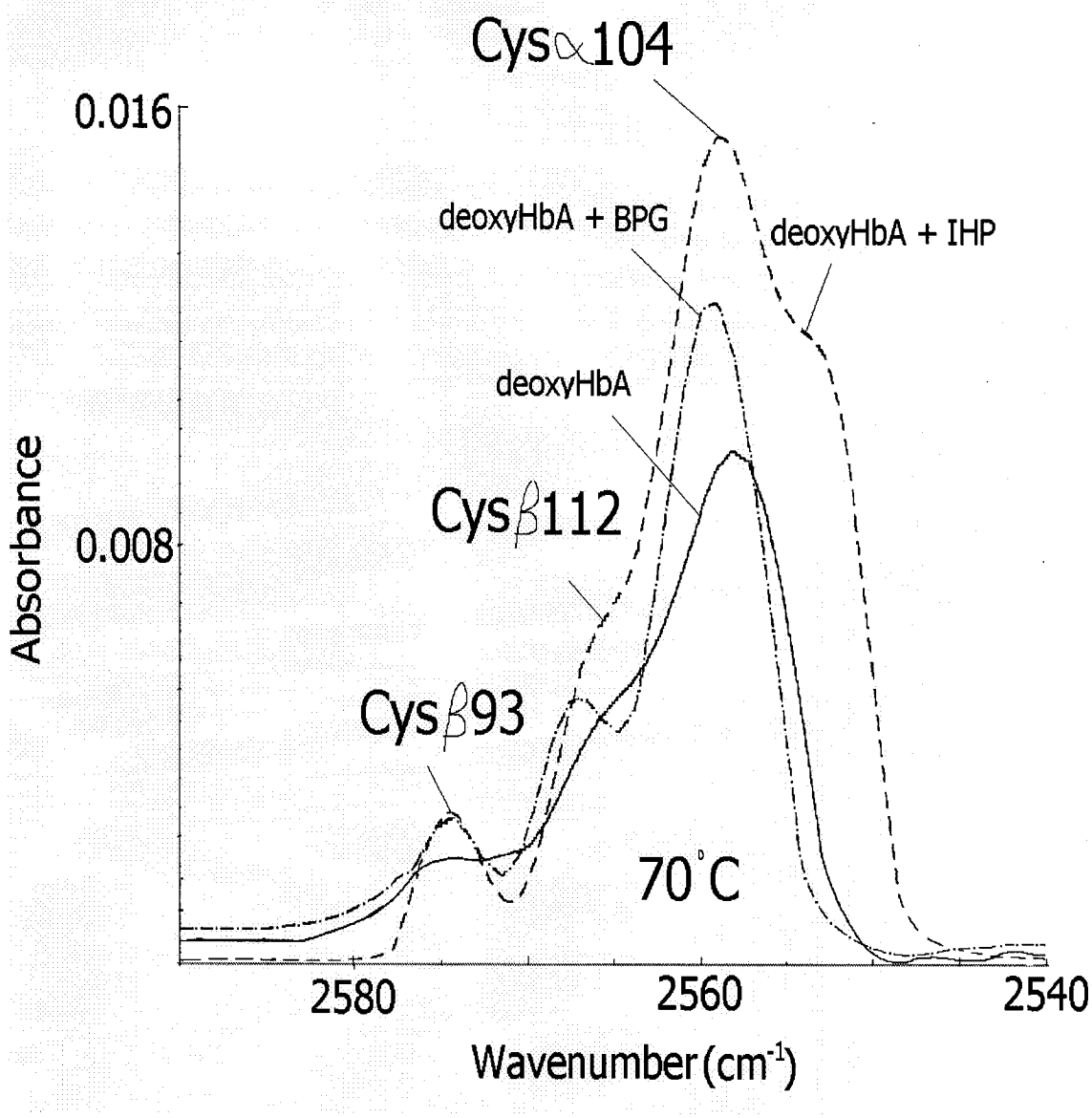

Fig 2.3: Effects of BPG and IHP binding on the ν(SH) absorbtion of 5.0 mM deoxyHbA in 0.2 mM NaPi buffer (pH 6.5) at 70°C. DeoxyHbA plus equimolar IHP (dashed line), deoxyHbA plus equimolar BPG (dotted-dashed line), and deoxyHbA (solid line). The experimental conditions are given in the legend of Figure 2.1.

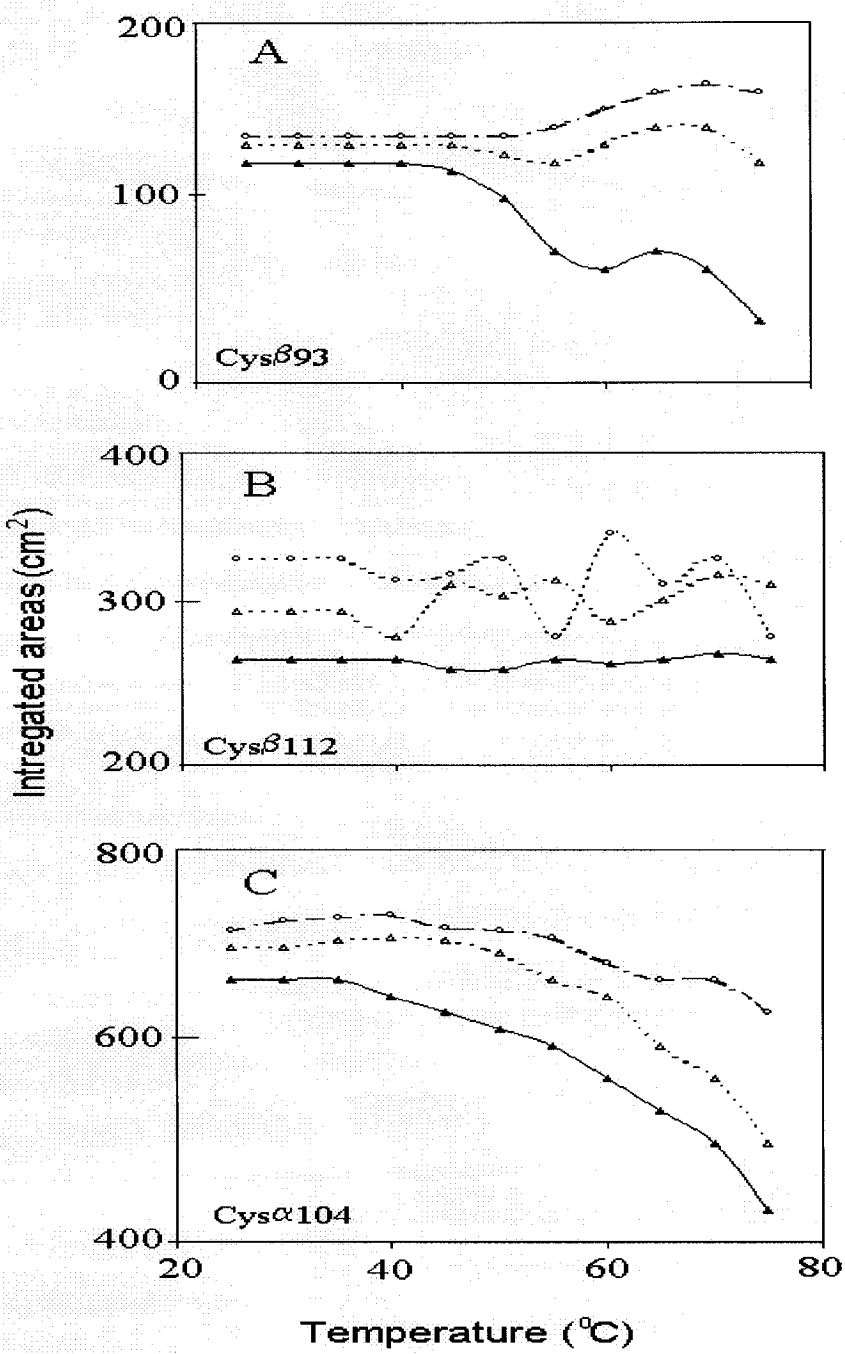

Fig 2.4: Plots of the integrated intensities of the ν(SH) bands of deoxyHbA with and without effectors *vs* temperature. DeoxyHbA (—▲—), deoxyHbA with BPG (--Δ--) and deoxyHbA with IHP (—○—). (A) ν(SH) intensity between 2575-2578 cm^{-1} corresponding to Cysβ93. (B) ν(SH) intensity between 2564-2567 cm^{-1} corresponding to Cysβ112. (C) ν(SH) intensity between 2556-2563 cm^{-1} corresponding to Cysα104.

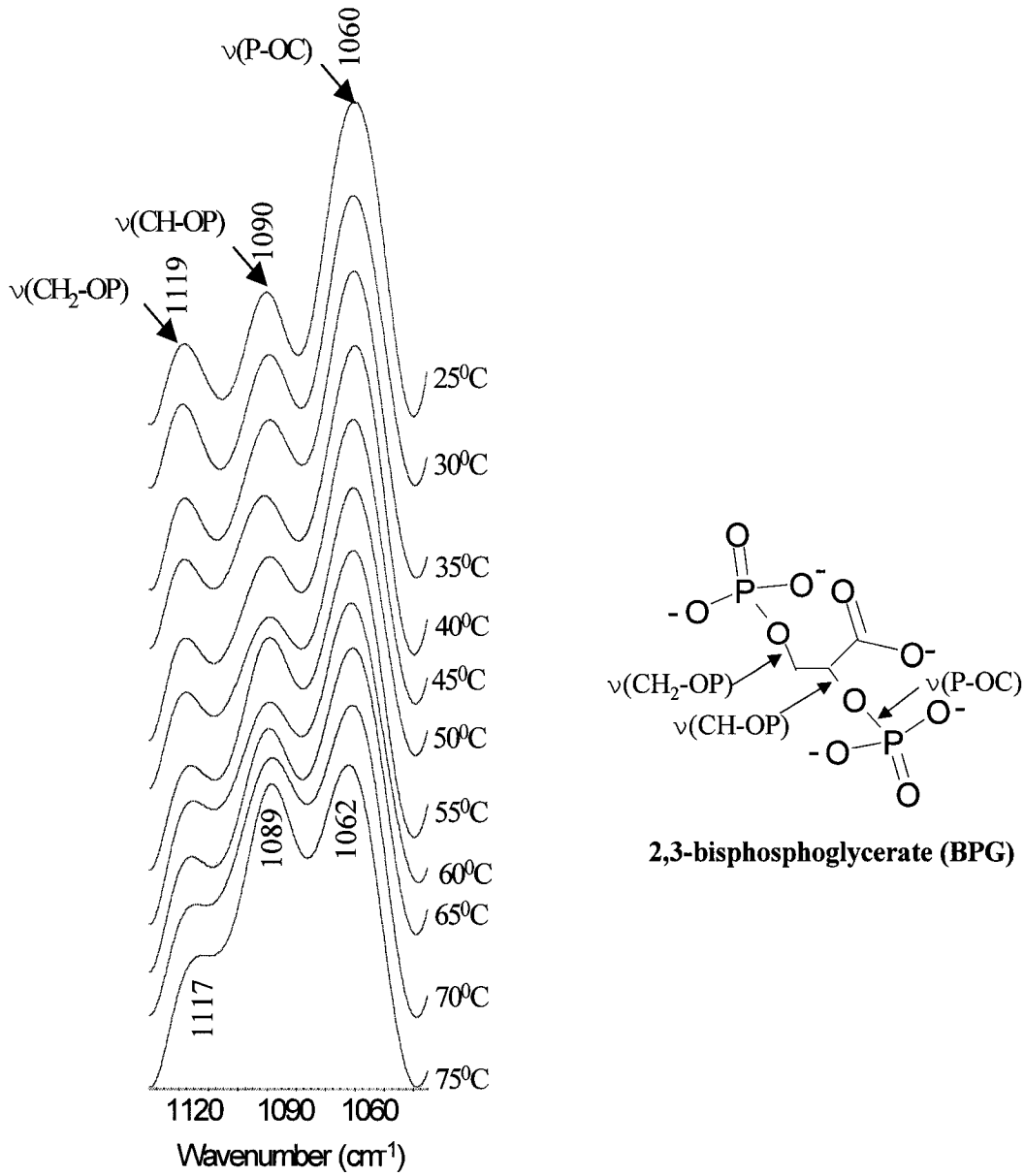

Fig 2.5: Effect of temperature on the FTIR spectra of 5.0 mM BPG in water at pH 3.8. The spectra were recorded in a 50-μm pathlength FTIR cell between 25°C and 75°C on a Nicolet IR-550 spectrometer using a MCT detector. The cell was equilibrated for 5 min at each temperature and the spectra are the average of 512 scans recorded with 2-cm^{-1} resolution. Background subtraction, baseline correction, smoothing and Fourier transform self-deconvolution were performed on the displayed spectrum (see text). The band assignments are based on those published for BPG at 20°C and pH 4-5 (15).

The effects of IHP on the thiol vibrations of deoxyHbA are similar but more dramatic than those of BPG. With increasing temperature, the Cysα104 peak at 2557 cm^{-1} is increasingly broadened by IHP and splits into two peaks at 2556 and 2562 cm^{-1} at 75°C (Figure 2.2). In the presence of BPG, the Cysα104 peak becomes narrower and blue-shifts to 2562 cm^{-1} with increasing temperature (Figure 2.3). The peak positions and intensities of the Cysβ112 absorption of the effector-bound forms of deoxyHbA fluctuate with temperature (Figure 2.4B), suggesting variation in the destabilizing effect of the effectors on the environment of Cysβ112. While the effectors induce changes in the hydrophobic environments of Cysα104 and Cysβ112, the Cysβ93 peak is intensified and remains stable over the temperature examined (Figures 2.2B,C and 2.4C). This suggests that effector binding has a stabilizing effect on the hydrophilic environment of Cysβ93 in deoxyHbA.

A plot of integrated ν(SH) band intensities *vs* temperature (Figure 2.4) reveals that the stabilizing or destabilizing effects of BPG are less pronounced than those of IHP. In the absence of BPG or IHP, the Cysβ93 peak intensity starts to decrease at 45°C and reaches a minimum at 60°C. In contrast, the ν(SH) absorption of Cysβ93 slightly diminishes between 50 and 55°C in BPG-deoxyHbA but increases again at 60°C, revealing dynamic changes in the Cysβ93 environment at high temperature. Although, effector-free deoxyHbA regains some Cysβ93 intensity at 65°C, it does not attain the initial value. However, the absorption of Cysβ93 increases at higher temperatures in effector-bound deoxyHbA and exhibits a maximum at 70°C, with considerable higher intensity than the effector-free form (Figure 2.4A).

The effector-bound forms of deoxyHbA display more fluctuations in Cysβ112 absorption with temperature than the free form (Figure 2.4B). This indicates increased environmental flexibility around Cysβ112 in the presence of the effectors as the temperature is varied. Fluctuating intensities were also observed for Cysα104 ν(SH) absorption in effector-bound deoxyHbA over the temperature range examined (Figure 2.4C). Combined these data suggest a destabilizing effect of the effectors on the hydrophobic environments of Cysα104 and Cysβ112 at the $\alpha_1\beta_1$ and/or $\alpha_2\beta_2$ interfaces.

Since the manufacturer advised to store BPG at 0°C (25), its thermal stability in water was probed by FTIR. Kempf and Zundel first studied the FTIR spectrum of BPG as a function of pH at room temperature (20°C) and assigned the bands (13,15). Five protons are released from the three acidic groups of BPG with increasing pH giving rise to the BPG pentaanion at high pH. The phosphate groups of BPG exhibits pK_a values of 2.2 (loss of $2H^+$), 7.1 and 7.5, and the pK_a of the carboxylic acid group is 3.7. Therefore, BPG exists largely as a tetraanion at physiological pH. At low pH an intramolecular hydrogen bond (COO^------$HOPO_2^-OC$) is formed between the carboxylate group and the phosphate group at position 2, which creates an asymmetric environment around the carboxylate group and $\nu_{as}(CO_2^-)$ appears at 1592 cm^{-1}. Breaking of the hydrogen bond at higher pH increases the symmetry and $\nu_{as}(CO_2^-)$ appears at 1583 cm^{-1}. Kempf and Zundel assigned bands at 1120, 1089 and 1055 cm^{-1} at pH 4-5 to $\nu(CH_2\text{-}OP)$ and ν(CH-OP) and ν(P-OC), respectively. The pH of BPG (5 mM) in water in our experiment was 3.8, which is very close to the pK_a (3.7) of the carboxylic acid group of BPG. The bands at 1119 and 1090 cm^{-1} closely match the values obtained by Kempf and Zundel (Table 2.1) for $\nu(CH_2\text{-}OP)$ and ν(CH-OP). However, they observed ν(P-OC) at 1055 cm^{-1} while we

observe it at 1060 cm^{-1} (Table 2.1). The discrepancy is likely due to the variation in the degree of H-bonding at pH 3.8 *vs* pH 4-5. The dramatic increase in the intensity of the 1090-cm^{-1} band at higher temperature reveals conformational change in the molecule on heating.

Table 2.2: FTIR bands (cm^{-1}) of BPG

Conditions	ν(P-OC)	ν(CH_2-OP)	ν(CH-OP)
pH 4-5, 20°C[b]	1055	1120	1089
pH 3.8, 25°C[a]	1060	1119	1090
pH 3.8, 75°C[a]	1062	1117	1089

[a] Observed values from Figure 2.5; [b] literature values from (15).

2.5 Discussion

The effects of BPG and IHP on the ν(SH) vibrations of deoxyHbA are attributable to changes in protein conformation around the cysteine residues. The binding of NO, CO and O_2 to the heme iron also significantly alters the thiol vibrations (19-20). The variations in the ν(SH) band parameters on ligand binding reflect differences in local environment and H-bonding experienced by the SH groups (22). The ν(SH) frequency increases with increasing thiol H-bond acceptor strength (22). In contrast, as the SH group becomes a stronger proton donor, the frequency of its ν(SH) absorption is lowered and intensified (22). Thus, the ν(SH) bandwidth is a measure of environmental mobility about the SH group. The more mobile the environment, the greater the expected bandwidth.

The ν(SH) band of Cysα104 in deoxyHbA is observed at higher wavenumber (2557 *vs* 2553 cm^{-1}) and with greater bandwidth than in heme-liganded (O_2, CO or NO) HbA indicating a less uniform environment for Cysα104 in deoxyHbA (20,22). On the other hand, the lower frequencies of Cysβ93 (2576 *vs* 2584 cm^{-1}) and Cysβ112 (2564 *vs* 2566 cm^{-1}) suggest that these SH groups are better H-bond donors in deoxyHbA than in the liganded forms (20,22).

The peak broadening effect of IHP on ν(SH) of Cysα104 of deoxyHbA (Figure 2.1) is indicative of a more flexible local environment in the presence of the effector. The crystal structure of oxyHb shows that the SH groups of Cysα104 are ideally positioned to form intrachain H-bonds with the peptide carbonyl oxygen of Leuα100 in the hydrophobic $\alpha_1\beta_1$ and $\alpha_2\beta_2$ interfaces (26). A frequency shift to higher wavenumber (2562 cm^{-1}) and the appearance of a shoulder at 2555 cm^{-1} (Figure 2.3) clearly demonstrates the disruptions of the $\alpha_1\beta_1$ and $\alpha_2\beta_2$ interfaces by IHP at high temperatures. BPG binding also broadens the Cysα104 peak at 25°C but narrows it at high temperature (Figures 2.1-2.3). Thus, the fluctuating bandwidth and frequency shifts to higher wavenumber reveal significant changes in the environment of Cysα104 on increasing the temperature.

The peak broadening effect of IHP on Cysα104 absorption could also be explained by the dissociation of tetrameric deoxyHbA into dimers with exposure of the $\alpha_1\beta_1$ interface to the bulk solvent at high temperature. Bare *et al.* showed that addition of guanidium chloride (GdnCl) or sodium dodesyl sulphate (SDS) to carbonmonoxyHbA broadened the ν(SH) absorption band of Cysα104 with increasing pH (19) suggesting the dissociation of HbA into α- and β- chains and exposure of the SH groups to the

exchanging solvent. On the basis of intensity measurements in small molecules, they attributed the large integrated ν(SH) absorption coefficients to the existence of highly polarized H-bonded SH groups in detergent and to the intact secondary structure of the G helices where Cysα104 is located. Since the guanidium ion can act only as a H-bond donor, Cysα104 must act as a H-bond acceptor under these dissociating conditions. The requirement of high pH (~12) to titrate the thiols in carbonmonoxyHbA in 6 M GdnCl reveals the persistence of strong H-bonding of SH groups in GdnCl. Bare *et al.* also reported that the relative integrated intensity of ν(SH) of ethane thiol (C_2H_5-SH) was 6 : 3 : 2 : 1 in H_2O, acetone, CCl_4 and dimethylacetamide, respectively, indicating the strong influence of H-bonding on the ν(SH) intensity. Figure 2.4 shows higher ν(SH) intensity for the three thiols in deoxyHbA on effector binding consistent with stronger H-bonding in the presence of these ligands.

The effectors broaden the ν(SH) absorption of Cysβ112 less than that of Cysα104 (Figures 2.1 and 2.3) suggesting that the Cysβ112 thiols are in a more stable environment. The crystal structure of oxyHb reveals that like Cysα104, Cysβ112 is located in a nonpolar region of the $\alpha_1\beta_1$ interface and seems to be involved in intrachain H-bond donation to the peptide carbonyl of Asnβ108 or Valβ109 (19, 22).

Studies of the dissociation of HbA in different solvents reveal that the deoxyHb tetramer is more stable than the heme-liganded Hbs. The sequence of decreasing stability of the tetramer is: deoxyHb > HbCO > HbO_2 ≅ metHbCN (28). This sequence is consistent with the fact that Hb dissociates into $\alpha_1\beta_2$ dimers and that the $\alpha_1\beta_2$ interface is stabilized by salt bridges between the C-termini of the subunits in the T structure (Table 1.2). Since the effectors favour the T structure over the R structure, they must further

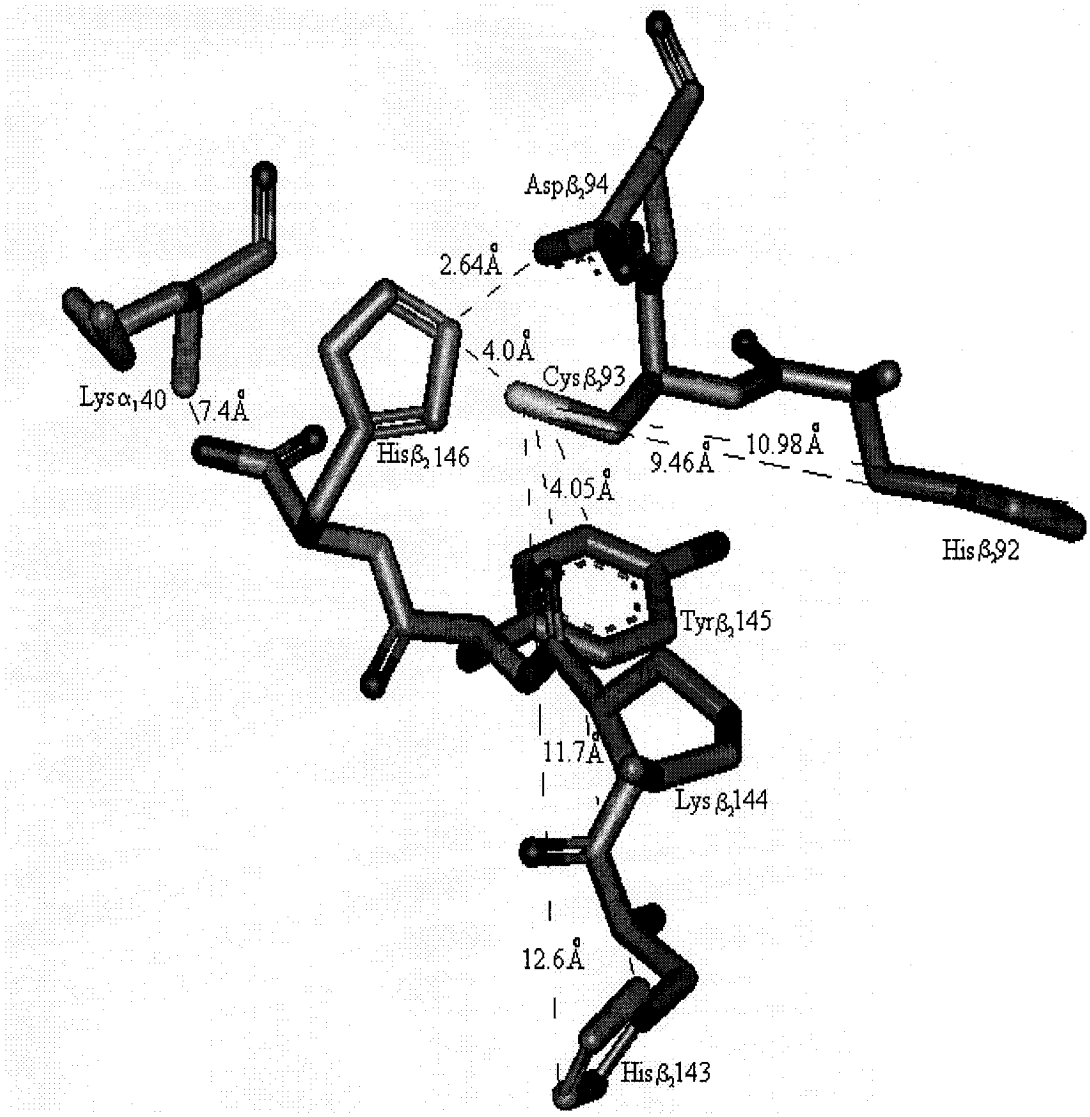

Fig 2.6: Crystal structure of deoxyHbA showing the environment of Cysβ93. The diagram was generated from PDB file 1gzx by WebLab Viewerlite. Atom CE1 of Tyrβ145 is 4.05 Å from SG atom of Cysβ93. Atoms ND1 and NE2 of Hisβ143 are 11.7 and 12.6 Å from atom SG of Cysβ93. Atoms ND1 and NE2 of Hisβ92 are 11.7 and 12.6 Å from SG atom of Cysβ93. Aspβ94 and Hisβ146 form a salt bridge that stabilizes the T structure of HbA (Table 1.2) and shields the surface-exposed sulfhydryl groups of Cysβ93. BPG forms a charged H-bond with the side chain of Hisβ143 (Table 1.2, Figure 1.5)

stabilize the $\alpha_1\beta_2$ interface and thus the polar environment of Cysβ93. This is reflected in the more intense and stable ν(SH) absorption of Cysβ93 in the presence of the effectors at high temperature (Figures 2.2-2.4).

The electronic stress that is generated on Hisβ143 on effector binding is transmitted to the polar environment of Cysβ93 in deoxyHbA through Lysβ144 and Tyrβ145. As shown in Figure 2.6, Hisβ143 is 11.7 Å from Cysβ93 with Tyrβ145 and Lysβ144 as intervening residues. Tyrβ145, the penultimate residue of the β-chain, has a strong influence on heme-heme interactions and on the environmental stability of Cysβ93 (27). Cysβ93 and Tyrβ145 are located in a pocket formed by the F and H helices in deoxyHbA and only 4.05 Å apart (Figure 2.6). According to Perutz *et al.* the side chain of Tyrβ145 has partial freedom in oxyHb but in deoxyHb it is firmly anchored in the pocket of F and H helices (26). HbA digested with carboxypeptidase A and lacking the final two β-residues (Tyrβ145 and Hisβ146) shows higher oxygen affinity and reduced cooperativity (n =1.3-1.5) compared to native HbA (n = 2.5-3.0).

3.0 BPG and IHP Stabilize the Heme Pocket and the Environment of the Aromatic Residues at the $\alpha_1\beta_2$ Subunit Interface in DeoxyHbA

3.1 Abstract

The effects of BPG and IHP on the heme pocket of deoxyHbA were studied by circular dichroism (CD) and unpolarized ultraviolet-visible (UV-vis) spectroscopy from 25 to 55°C with a temperature interval of 5°. The Soret CD band of 0.5 mM deoxyHbA was detected at 418 and 432 nm with ellipticities of –2.4 and +28 $M^{-1}cm^{-1}$ at 25°C. In the presence of a 2-fold molar excess of BPG or IHP, deoxyHbA exhibited a similar Soret band but the positive ellipticity at 432 nm was intensified by 2-4 units. While the intensity of the Soret CD absorption of effector-free deoxyHbA decreased with increasing temperature, the Soret CD absorption of effector-bound deoxyHbA was intensified by 2-5 units with temperature. At 55°C ~50% loss of the Soret CD absorption was observed in free deoxyHbA but not in effector-bound deoxyHb demonstrating a marked stabilizing effect of the effectors on the heme environment of ligand-free HbA. The negative trough at 418 nm disappeared fully and the Soret band blue-shifted without the effectors. Much less dramatic effects of BPG or IHP on the unpolarized Soret absorption of deoxyHbA were observed by UV-vis at 25°C. However, 10-12% loss of the Soret band absorption was found at 55°C in the absence of the effectors.

The effects of BPG and IHP on the near-UV CD bands of deoxyHbA were also evaluated at a physiologically relevant concentration (3 mM) for the first time. The 287-

nm negative CD band, which has long been used as a T-state CD marker, was 15-20% intensified by the effectors at 25°C. The effectors had little influence on the 260-nm band, which is assigned to heme absorption, at room temperature. However, at 45°C, effector-free deoxyHbA exhibits five valleys instead of the characteristic three valleys of the 260-nm CD band, and loses the smooth shape of the 287-nm band. The combined spectroscopic data demonstrate that effector binding significantly stabilizes the environment of the heme pocket as well as certain aromatic residues in deoxyHbA.

3.2 Introduction

CD can be used to investigate the structural organization of protein molecules (30-35). In addition to the protein moiety, hemoglobin (Hb) contains hemes with strong electronic transitions that are extremely sensitive to the surrounding environment and ligand binding at the heme iron. The presence of hemes in the protein offers three distinct spectral regions of investigation, each containing information on the structural organization of the Hb molecule. In the far-UV region (190-240 nm), the predominant chromophores are the peptide groups, which provide information regarding the three-dimensional organization of the molecule. The predominant chromophores in the near-UV region, which extends from 240-300 nm, are the side chains of aromatic amino acid residues. These are extremely sensitive to local environmental changes due to polypeptide chain-chain interactions. No amino acid chromophores absorb above 300 nm. The CD spectra of the heme transitions that occur in the visible region are governed by the environmental asymmetry of the globin moiety (29).

The allosteric transition of the tetrameric respiratory protein, Hb, from the low affinity deoxy or T (tense) state to the high affinity oxy or R (relaxed) state with rising

oxygen saturation is accompanied by a change in quaternary and tertiary structures as dicussed in Chapter 1 (1-6,8-13,29-31). The amino acid residues that are located at the $\alpha_1\beta_2$ interface experience a large change in their relative orientations and environments (1-6,8,27, 29-33). The $\alpha_1\beta_2$ interface of HbA contains 19 amino acid residues with critical contacts of ~34 atoms between the C helix of one chain and the FG corner of another (36). Four aromatic residues, namely Tyrα42, Tyrα140, Trpβ37 and Tyrα145, are of particular interest because of their contributions to the near-UV CD absorption (33).

Perutz *et al.* reported large changes in the near-UV CD spectra of oxy- and deoxyHbA, particularly in the regions centered at 260 and 287 nm. They observed that deoxygenation of Hb is accompanied by a large decrease in the positive CD band at 260 nm and the appearance of a negative band at 287 nm. They assigned the 260-nm band to the hemes and the 287-nm negative band to both hemes and aromatic residues (3, 4). Later, Baldwin *et al.* suggested that Tyrα42 and Trpβ37 are responsible for the negative band at 287 nm (34), and Li *et al.* have more recently shown that Trpβ37 and Tyrα140 contribute 26% and 30%, respectively, to this negative band in deoxyHbA (31).

The allosteric effectors, BPG and IHP, which favour the T structure over the R structure, should have a dramartic influence on the environment of the heme pocket. This is investigated here by CD and UV-vis spectroscopy. The tharmal stability of the near-UV CD bands of deoxyHbA in the presence of BPG and IHP were investigated to extract information regarding the influence of the effectors on the $\alpha_1\beta_2$ interface of HbA.

3.3 Experimental Procedures

3.3.1 Materials

The materials used are listed in Section 2.3.1.

3.3.2 Methods

Hb, BPG and IHP stock solutions were prepared as described in Section 2.3.2. In order to study the Soret CD band, a 1-μL aliquot of 100 mM BPG or IHP was added to 17 μL of 3.0 mM deoxyHbA and diluted to 100 μL with 0.2 M degassed NaPi buffer (pH 7.0) in a glove box (Mbraun-Unilab). To examine the influence of the effectors on the near-UV CD spectra of deoxyHbA, a sample was prepared by adding 5 μL of 100 mM BPG or IHP to 80 μL of 3.0 mM (tetramer) deoxyHbA inside the glove box. The control was prepared by adding an equivalent amount of buffer to the deoxyHbA solution. A 20-μL aliquot of effector-bound or free deoxyHbA was loaded onto the windows of an FTIR cell equipped with a temperature-controlled cell mount (Harrick) and two 13 × 2 mm CaF_2 windows separated by 50-μm spacer. The cell was quickly assembled and the spectra were recorded on a JASCO CD 710 spectropolarimeter between 25°C and 55°C with a temperature interval of 10°. At each temperature, the cell was equilibrated for 5 min and each spectrum is an average of 10 scans with a resolution of 0.2 nm, a response time of 4 s, a scan speed of 10 nm/min and a bandwidth of 1 nm. The IR cell temperature was controlled using an Omega CN8500 temperature controller and monitored with a thermocouple placed in close proximity to the CaF_2 windows. The contributions from buffer, IHP and BPG were subtracted from the spectra using JASCO CD software. The ellipticities of all bands are expressed in molar CD, $\Delta\varepsilon$ (M^{-1} cm^{-1}). The UV-vis spectra were also recorded in the FTIR cell on a Beckman DU 650 UV-vis spectrometer equipped with a custom-made bracket to hold the FTIR cell. Data analysis was performed using Sigma Plot and Microsoft Excel software.

3.4 Results

The Soret CD band of 0.5 mM deoxyHbA exhibited an intense peak at 432 nm with a positive ellipticity of ~28 $M^{-1}cm^{-1}$ and a negative trough at 418 nm with an ellipticity of ~2.4 $M^{-1}cm^{-1}$ at 25°C (Figure 3.1). These characteristics of the Soret band of tetrameric deoxyHb were previously reported by a number of investigators (30,34,35). In the presence of a 2-fold molar excess of BPG or IHP, deoxyHbA exhibited a similar Soret band but the positive ellipticity at 432 nm was intensified by 2-4 units, reflecting an influence of the effectors on the heme environment. In the absence of the effectors, the intensity of the Soret CD band decreased with increasing temperature. However, no loss of intensity was observed in the presence of the effectors. In fact, the absorption at 432 nm was intensified by 2-5 units in effector-bound deoxyHbA at 55°C, whereas free deoxyHbA lost ~50% of its Soret CD absorption (Figure 3.1). Moreover, the negative trough at 418 nm fully disappeared and a positive trough developed at 415 nm without the effectors. The Soret (432 nm) band of free deoxyHbA also blue-shifted to 430 nm.

BPG or IHP had little effect on the unpolarized Soret band of deoxyHbA as observed by UV-vis at 25°C. DeoxyHbA exhibited identical Soret absorption at 430 nm in the presence and absence of the effectors at room temperature (Figure 3.2). However, at 55°C, effector-free but not effector-bound deoxyHbA lost ~10-12% absorption at 430 nm confirming the stabilizing influence of the effectors at the higher temperature.

The effects of BPG and IHP on the near-UV CD band of 3 mM deoxyHbA solutions were examined. This is the first time that the spectra were recorded at close to the physiological concentration. The 287-nm negative CD band, which has long been used as a T-state CD marker of HbA (3, 4, 30, 31), was 15-20% intensified with the effectors

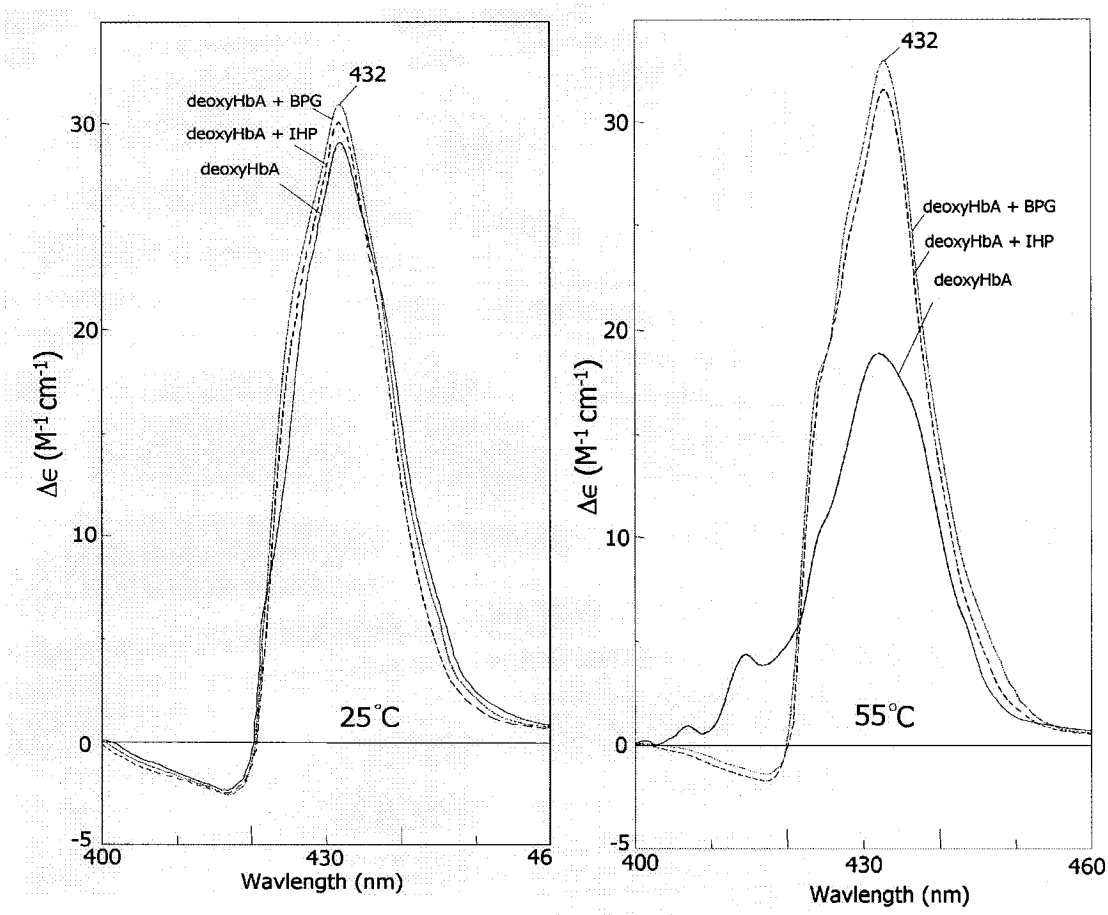

Fig 3.1: Effects of BPG and IHP on the Soret absorption of 0.5 mM deoxyHbA in 0.2 M NaPi buffer (pH 7.0) at 25 and 55°C. Shown are deoxyHbA (solid line), deoxyHbA plus 2x BPG (dotted line) and deoxyHbA plus 2x IHP (dashed line). The spectra were recorded in a 50-μm pathlength FTIR cell on a JASCO CD 710 spectropolarimeter with a scan speed of 20 nm/min, a response time of 2 s and a slit of 0.2 nm. Each spectrum is the average of 10 scans. At each temperature the cell was equilibrated for 5 min. Contributions from buffer, BPG or IHP were subtracted from the respective spectra. All calculations and analysis were performed using the JASCO CD software.

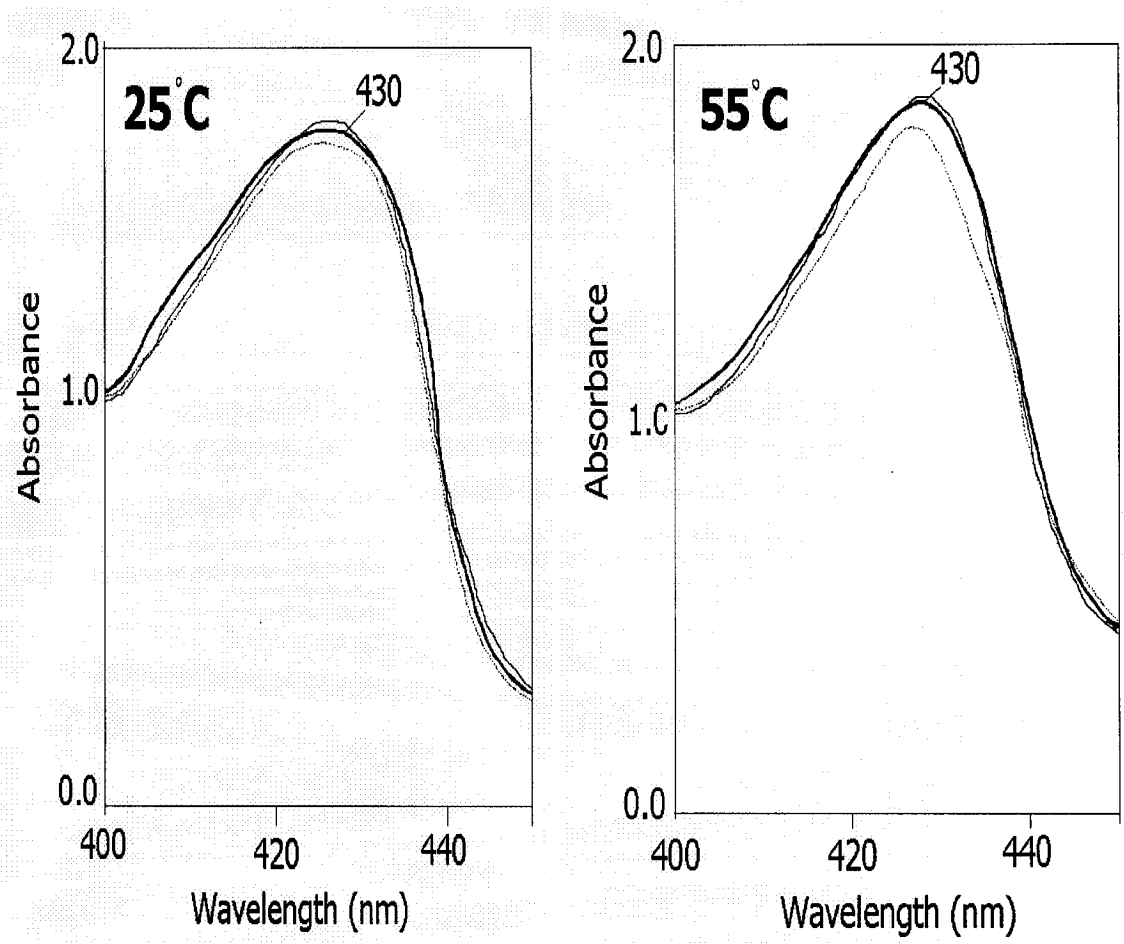

Fig 3.2: Effects of BPG and IHP on the unpolarized Soret absorption of 0.5 mM deoxyHbA in 0.2 M NaPi buffer (pH 7.0) at 25°C and 55°C. Shown are deoxyHbA plus 2x IHP (thin solid line), deoxyHbA plus 2x BPG (bold solid line) and deoxyHbA (dotted line).The spectra were recorded in 50-μm pathlength FTIR cell on a Beckman DU 650 UV-vis spectrophotometer at a scan rate of 6 nm/min. The cell was equilibrated for 5 min at each temperature before recording the spectra. Contributions from buffer, BPG and IHP were subtracted from the respective spectra.

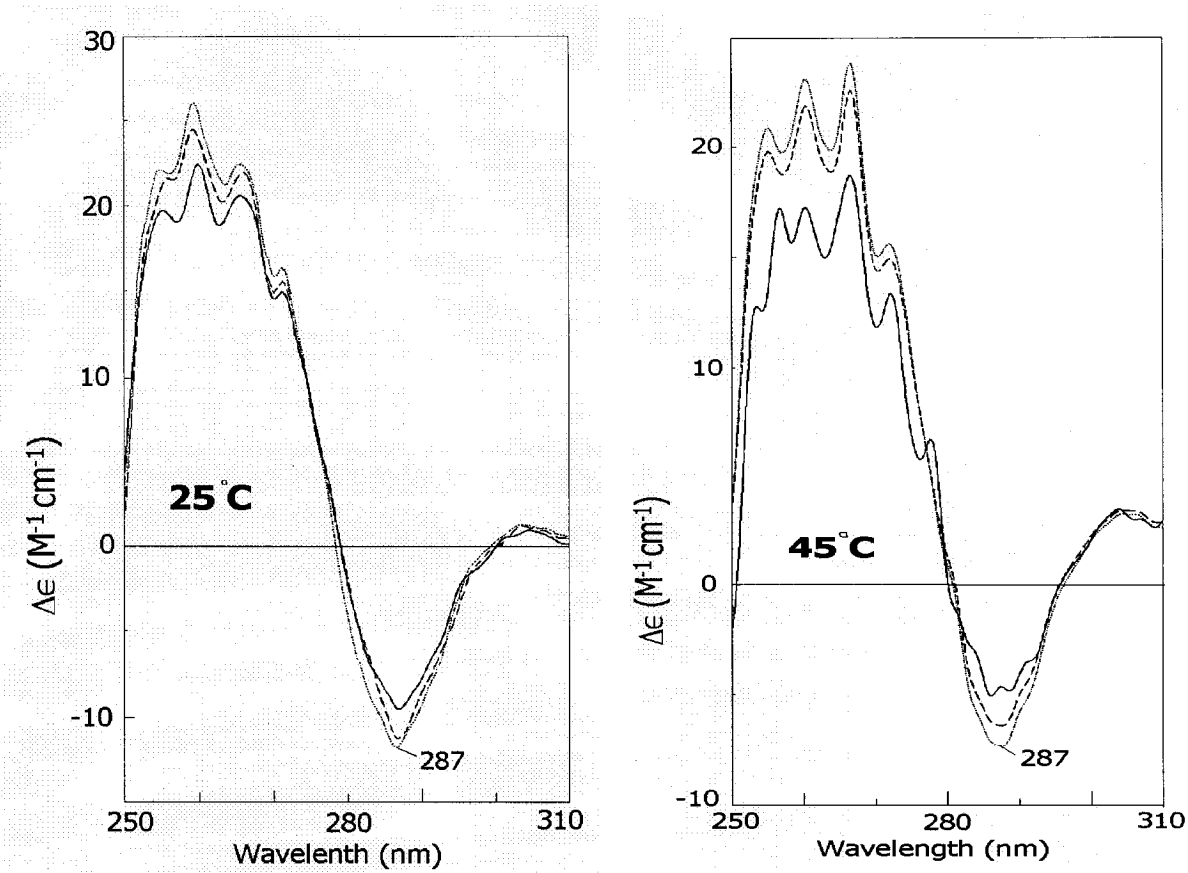

Fig 3.3: Effects of BPG and IHP on the near-UV CD spectra of 3.0 mM deoxyHbA in 0.2 M NaPi buffer (pH 7.0) at 25 and 45°C. Shown are deoxyHbA (solid line), deoxyHbA plus 2x BPG (dashed line), deoxyHbA plus 2x IHP (dotted line). The spectra were recorded in 50-μm pathlength FTIR cell on JASCO CD 710 spectropolarimeter. Each spectrum is the average of 10 scans with a scan speed of 20 nm/min, a slit of 0.2 nm and a response time of 2 s. Contributions from buffer, BPG and IHP were subtracted from respective spectra.

present at 25°C (Figure 3.3). Approximately 50% of the intensity of this band is attributed to heme absorption and ~50% to the absorption of aromatic residues, particularly Trpβ37 and Tyrα140, at the $\alpha_1\beta_2$ subunit-interface (3, 4, 30, 31). No dramatic effects of the effectors on the 260-nm band, which was assigned to the heme absorption by Perutz *et al.*, were observed at room temperature. However, effector-free deoxyHbA exhibits a five-valley spectrum instead of a three-valley one between 250-280 nm (30, 31) and loses the smooth shape of the 287-nm band at 45°C. When the temperature was increased above 50°C, both effector-bound and effector-free deoxyHbA exhibited multiple valleys in this spectral region (data not shown). These combined spectral changes demonstrate that the effectors stabilize the environment of heme pocket as well as aromatic residues at the $\alpha_1\beta_2$ interface in T state HbA.

3.5 Discussion

The CD spectra in the Soret, visible and near-UV regions may reflect conformations related to the functional properties of Hb (34). The C-terminal residues of both the α- and β-chains have a profound effect on the Soret absorption and functional properties of all mammalian deoxyHbs (30-32, 34-37). The C-terminal residues affect heme-liganded Hbs to a lesser extent. Tyrβ145 and Hisβ146 are far from the heme (26) but removal of these residues by limited carboxypeptidase A digestion induces drastic changes in the oxygen binding properties and the Soret CD absorption of deoxyHbA (34). For example, carboxypeptidase A-digested HbA without Tyrβ145 and Hisβ146 exhibited ~8-fold higher oxygen affinity and ~50% reduced cooperativity (Hill coefficient, n = 1.2) than the native protein. The Soret CD absorption was 30% reduced and blue-shifted in the deoxy form but remained unaffected in the oxy form (29, 34). The α-helical content remained

unchanged as reflected by the constant magnitudes of the negative CD trough at 222-nm. Similar properties are exhibited by Hb Rainier, Hb Bethesda and Hb Nancy, where cysteinyl, histidyl and aspartyl residues replace Tyrβ145, respectively (27, 32).

Replacement of the α-chain C-terminal residues, which also play an important role in the allosteric transition, has less effect on the properties of mammalian Hbs. Hb Rouen, a Tyrα140→His variant, was found in a French family with polycythemia disease. This Hb variant exhibits moderately higher oxygen affinity and reduced cooperativity (n = 2.1) than HbA. However, Hb Suresnes, where Argα141 is replaced by a histidyl residue, and other variants of Argα141 show very high oxygen affinity and decreased cooperativity (32).

Salts that participate in the T-state-stabilizing electrostatic networks should have a profound influence on the properties of Hb. Sugita *et al.* observed that deionization of Hb increases its O_2 affinity and addition of an equivalent amount of BPG restores it to the normal value (34). Deionization also affects the Soret CD absorption of deoxyHb. The positive ellipticity of the Soret band of deoxyHb was decreased by ~30% upon deionization and it was restored to the normal value upon addition of equimolar BPG. The partial oxygen pressures required for 50% O_2 saturation of native Hb, deionized Hb and deionized Hb with equimolar BPG were 8.4, 3.2 and 8.3 mm Hg, revealing the extraordinary influence of BPG on the stability of the T structure (34).

The heme Cotton effect originates from $\pi \rightarrow \pi^*$ transitions and is affected by a number of factors including the oxidation state of hemes, ligand binding, chain-chain interactions and the side chains of aromatic residues (29, 32). According to the theoretical model of Hsu and Woody, the major contributions to the heme optical activity arise from coupling

heme $\pi \rightarrow \pi^*$ transitions with $\pi \rightarrow \pi^*$ transitions of nearby aromatic residues (29, 32, 38). The authors predicted the involvement of aromatic residues that are within 12 Å of the heme. Of the 21 aromatic residues in the α-chain, 7 (Hisα58, Pheα33, Pheα43, Pheα98, Tyrα42, Tyrα140 and Trpα14) were found at a distance where interactions could impart significant rotational strength to the heme transitions. Of the 22 aromatic residues in the β-chain, 9 (Hisβ63, Hisβ69, Pheβ41, Pheβ42, Pheβ71, Pheβ85, Pheβ103, Tyrβ130 and Trpβ15) were suggested to be important in these interactions. The proximal Hisα87 and Hisβ92 ligands were suggested to contribute little to the rotational strength of the heme. Due to their strongly allowed transitions in the far-UV, tyrosine and tryptophan residues within 10-15 Å distance interact strongly with the hemes providing significant rotational strength to the heme transitions (29, 32, 38). The variations in the Soret CD absorption in Hb Rouen (Tyrα140→His), Hb Bethesda (Tyrβ145→His), Hb Rainier (Tyrβ145→Cys) and Hb Nancy (Tyrβ145→Asp) are probably due to variation in coupling with the heme transitions.

The $\alpha_1\beta_2$-subunit interface plays a dominant role in the properties of Hb, especially in the deoxy state. The crystal structure shows that this interface is comprised of 19 residues with critical contacts between the C helix of one chain and the FG corner of another (26, 33, 36). Trpβ37, which contributes to the UV CD absorption, particularly to the 287-nm negative band in deoxyHbA (Figure 3.3), is located on the C helix (C3), which has a marginal tendency to be helical (36). The indole ring of Trpβ37 forms a hydrogen bond with the carboxylate of Aspα94, which is considered to stabilize the T-state and is broken on oxygenation (30). Hb Rothschild (HbR^1; Trpβ37→Arg) exhibits a K_D for tetramer dissocation into dimers (2.5×10^{-4} M) 2-fold greater HbA (36). Destabilization of the

HbR^1 tetramer is unlikely due to electrostatic repulsion, since Aspα94 in the vicinity Argβ37 should favour electrostatic attraction. Also Hb Hirose (Trpβ37→Ser) has a stronger dissociation tendency than HbA (30, 31) but here the substitution is by a neutral serine. The destabilization of the $\alpha_1\beta_2$ interface in the Trpβ37 mutants could be explained by the interruption of a pattern of hydrophobic residues, which is required for the correct folding and stability of $\alpha_1\beta_2$ interface. Additional requirement for the hydration of Argβ37 in HbR^1 may force greater solvent exposure of its $\alpha_1\beta_2$ interface than that of HbA (36).

Four aromatic residues (Tyrα42, Tyrα140, Tyrβ145 and Trpβ37) located at the $\alpha_1\beta_2$ interface contribute to the near-UV CD spectral changes in the 270-290 nm region in oxy- and deoxyHb (29-31). The H-bonding character of Trpβ37 and its consequences are discussed above. The crystal structure shows that Tyrα140 forms an intrasubunit H-bond with the peptide carbonyl of Valα93 (Table 1.2) and has some contacts with the β subunit in deoxyHbA (30, 39). N-stearyl-L-Tyr ester in methylcyclohexane exhibits two CD peaks at 277 and 283 nm. However, addition of the H-bonding agent, N, N-dimethylacetoamide, red-shifted the peaks to 280 and 286 nm (40). These peaks are also found in the difference CD spectra of deoxyHbA and Hb Rouen (Tyrα140 → Ser) suggesting that Tyrα140 is H-bonded in deoxyHb, which stabilizes the T structure (30).

Tyrα42 and Tyrβ145 form interchain H-bonds with Aspβ99 and Valα98, respectively (Table 1.2), and supposedly stabilize the T structure (3, 4, 30). Hb Kemsey (Aspβ99→Arg) is characterized by high O_2 affinity and reduced cooperativity (41). Addition of IHP to Hb Kemsey partially restores the cooperativity and the negative CD band at 287 nm (3, 41), which suggests that the H-bond between Tyrα42 and Aspβ99

contributes little to the 287-nm band (30). Li *et al.* recently showed that Tyrα140 and Trpβ37 make 30% and 26% contributions to this band and also suggested the involvement of other aromatic residues (Tyrα42 and Tyrβ145) at the $\alpha_1\beta_2$ interface (30).

Hisβ146, which forms salt bridges with the carboxylate of Aspβ94 and the amino group of Lysα40 and screens the S-H group of Cysβ93 in the T structure, is another candidate stabilizer of the $\alpha_1\beta_2$ interface. HbA devoid of the C-terminal Hisβ146 shows identical absorption and CD spectra to those of native HbA. However, the Soret CD band of HbA devoid of both Hisβ146 and Tyrβ145 is blue-shifted with a lower molar ellipticity with respect to native HbA (29, 42). The blue-shifted and ~50% reduced Soret CD absorption of HbA without effectors at 55°C (Figure 3.1) is indicative of loss of the salt bridges and H-bonds formed by Hisβ146 and Tyrβ145. In the presence of BPG and IHP, deoxyHbA retains its Soret CD intensity with increasing temperature reflecting the integrity of C-terminal β-chain interactions at 45°C (Figure 3.1). The stabilization of the FTIR ν(SH) absorption of Cysβ93, the 287-nm CD of aromatic residues, which are all located at the $\alpha_1\beta_2$ interface, by BPG and IHP (Chapter 2) suggests that the effectors stabilize the heme pocket by stabilizing the $\alpha_1\beta_2$ interface in T state HbA.

The CD spectra of isolated chains of HbA are different from those of tetrameric HbA in the Soret and near-UV regions (31,35). The arithmetic mean of the Soret bands of the isolated α- and β-chains is almost the same as that of the tetramer in the oxy forms but ~50% less intense than the tetramer in the deoxy forms (35). The retention of Soret intensity at 55°C in the presence of effectors suggests that these ligands stabilize the deoxyHbA tetramer. Above 55°C the tetramer may dissociate into monomers or dimers

since the Soret absorption is quickly lost (data not shown) even in the presence of the effectors.

The arithmetic mean of the near-UV CD spectra of the isolated oxy α- and β-chains in the 280-300 nm region is also identical to the spectrum of oxyHbA but significantly different from that of deoxyHbA (31). This reveals changes in the environments of the aromatic residues on deoxygenation of the tetramer. Recently, Li *et al.* showed that the environment of aromatic residues in the $\alpha_1\beta_2$ interface is equally affected by changes in tertiary and quaternary structures upon deoxygenation (31). The 15-20% increased intensity of the 287-nm negative CD band upon BPG and IHP binding to deoxyHbA reveals that the effectors further alter the tertiary and/or quaternary structure of the deoxy protein and thus the environment of the aromatic residues that contribute to the 287-nm absorption.

4.0 BPG and IHP Destabilize Secondary Structures in DeoxyHbA

4.1 Abstract

The effects of BPG and IHP on the secondary structure of adult human deoxyhemoglobin (deoxyHbA) were studied by Fourier transform infrared (FTIR) and circular dichroism (CD) spectroscopies between 25 and 95°C with a temperature interval of 5°. Bands in the amide I′ region (1700-1600 cm^{-1}) were observed at 1608, 1623, 1635, 1653, 1668 and 1675 cm^{-1} in the Fourier self-deconvolved and second-derivative FTIR spectra of 3 mM deoxyHbA in the presence and absence of the effectors. The intensities of the two prominent bands at 1653 and 1635 cm^{-1}, which are assigned to α-helical and turn absorption, respectively, decreased with increasing temperature. Two strong bands at 1617 and 1684 cm^{-1} appeared at high temperature and correspond to intermolecular antiparallel β-sheet absorption due to aggregation. Plots of intensity *vs* temperature revealed that the loss of α-helices and the appearance of aggregation occur in three distinct phases. In the presence of effectors, the plots shifted by 5-15°C to lower temperature, revealing that effectors destabilize the secondary structure of deoxyHbA.

The far-UV CD of 0.5 mM deoxyHbA at 25°C exhibited two negative peaks, typical of α-helices, at 208 and 222 nm with ellipticities of -530 and -640 $M^{-1}cm^{-1}$, respectively. With the rising temperature, the negative ellipticity at these wavelengths decreased reflecting the loss of α-helices on heating. A plot of the intensity at 222 nm *vs*

temperature reveals 26, 47, 67 and 88% loss of α-helices at 45, 55, 65 and 75°C, respectively.

4.2 Introduction

In Chapters 2 and 3, the effects of BPG and IHP binding on the cysteine and aromatic residues, and on the heme pockets of deoxyHbA were reported. In this chapter, their effects on the secondary structures of deoxyHbA are examined. DeoxyHb is a weaker acid than oxyHb and this phenomenon, known as the Halden effect, is attributed to changes in secondary structure that expose different residues to the bulk solvent in the oxy and deoxy protein (17, 18). Convincing evidence to support this hypothesis has not been published so far (17,18).

Hydrogen-tritium labelling revealed that some of the peptide protons of deoxyHbA display a large increase in exchange rate following oxygenation and allosteric transition (43). It is reported that there are five sets of peptide protons (each consisting of 4 to 18 protons) and all the protons in a set exchange at the same rate in deoxyHb. When deoxyHb is liganded, all the protons in a set move to a new rate that is faster by factors ranging from 14- to 10^4-fold. The differences in exchange rate are attributed to a transient local unfolding of individual structure segments, involving the breaking of a number of H-bonds and exposure of the hydrogens to the solvent. Since the mechanism of unfolding of individual segments depends on the ligand states of Hb, deoxygenation should have an effect on the secondary structure of Hb.

X-ray crystallographic studies do not reveal changes in secondary structure on deoxygenation. However, both spectroscopic and X-ray crystallographic studies have indicated large differences between tertiary and quaternary structures of oxy- and

deoxyHbA (26,30,39). The three-dimensional structures derived from X-ray crystallography reflect a static picture of the crystalline state of the protein that lacks dynamic and functional information. The structural data need to be complemented by spectroscopic studies in solution where proteins maintain their native conformations.

Fourier transform infrared (FTIR) and far-ultaviolet circular dichroism (far-UV CD) spectroscopies are widely used to study the secondary structure of polypeptides and proteins in solutions. The amide I vibrational mode of proteins with IR absorption between 1600-1700 cm^{-1} consists of 80% peptide C=O (carbonyl) stretching co-ordinate, with further contributions from C-N stretching and N-H deformation co-ordinates (44-48). This mode is very sensitive to the backbone conformation and degree of hydrogen bonding of the peptide carbonyls (45,46). However, strong absorption of H_2O in this region masks the amide I mode but this shortcoming can be overcome by dissolving the proteins in deuterium oxide (D_2O), which is transparent in this spectral region. The amide I bands in D_2O downshift by 2-5 cm^{-1} and are designated amide I′ (44-45).

4.3 Experimental Procedure

4.3.1 Materials

The materials used are listed in Section 2.3.1.

4.3.2 Methods

Stock solutions of BPG, IHP and deoxyHbA and were prepred in D_2O as described in Section 2.3.2. To allow H/D exchange the protein was left standing at 4°C for 12-18 h. A 5-μL aliquot of 100 mM BPG or IHP was added to 100 μL of 3.0 mM (tetramer) deoxyHbA inside the glove box (Mbraun-Unilab). The HbA sample (25 μL), prepared in this way, was loaded onto a window of an FTIR cell equipped with a temperature-

controlled cell mount (Harrick) and two 13 × 2 mm CaF_2 windows separated by a 50-μm spacer. The cell was assembled immediately inside the glove box. A control was prepared by adding 5 μL of NaPi buffer (pD 7.4) to 100 μL of 3.0 mM deoxyHbA. The spectra were recorded from 25 to 95°C with a temperature interval of 5° on a Nicolet Magna IR 550 Series II FTIR spectrometer equipped with a deuterated triglycine sulfate (DTGS) KBr detector and purged with dry air from a Whatman FTIR Purge Gas Generator (Model 75-52). At each temperature, the cell was equilibrated for 5 min and each spectrum is an average of 512 scans with a resolution of 2 cm^{-1} and an aperture of 69. The IR cell temperature was controlled using an Omega CN8500 temperature controller and monitored with a thermocouple placed in close proximity to the CaF_2 windows. Omnic (Nicolet) software was used to subtract contribution of the buffer, BPG and IHP from the spectra. Fourier self-deconvolution (FSD) was performed using a band width of 25 cm^{-1} and a resolution enhancement factor (K) of 1.4 in a Happ-Ganzel window. The second derivative spectra were obtained by using a power of 3 and a break point of 0.3.

The far-UV CD spectra of 0.5 mM deoxyHbA in 0.2 M NaPi buffer (pH 7.4) were also recorded in the FTIR cell (Harrick) with a 50-μm pathlength on a JASCO 710 spectropolarimeter. Each spectrum was an average of 10 scans recorded with a scan speed of 20 nm/min, a response time of 2 s and a slit of 0.2 nm. Buffer contributions were subtracted from each spectrum using the JASCO CD software. At each temperature, the IR cell was equilibrated for 10 min and the temperature was controlled as described above for the FTIR experiments.

4.4 Results and Discussion

The secondary structure of HbA as deduced from crystallographic data is

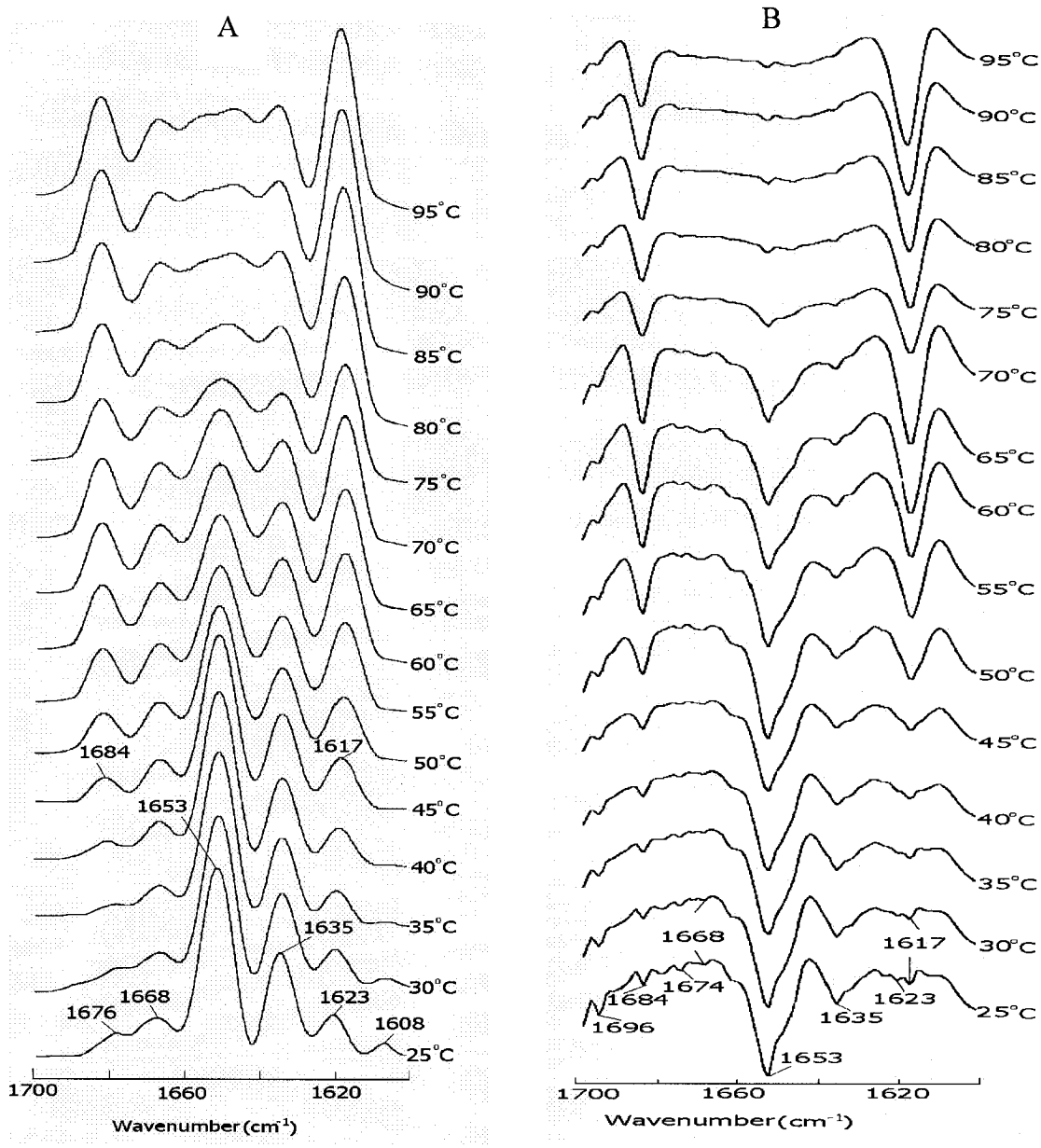

Fig 4.1: FTIR spectra of 3 mM deoxyHbA in 0.2 M NaPi buffer (pD 7.4) in the amide I′ (D_2O) region *vs* temperature. Fourier self-deconvolved (FSD) (A) and second derivative (SD) (B) spectra are shown. The spectra were recorded with a 50-μm pathlength. At each temperature the cell was equilibrated for 5 min and each spectrum is an average of 512 scans recorded with a resolution of 2 cm^{-1}. Contributions from buffer were subtracted from the corresponding spectrum. Fourier self-deconvolution was performed with a HWHH of 25 cm^{-1} and a K factor of 1.4, and the second derivative spectra were obtained with a power of 3 and break point of 0.3.

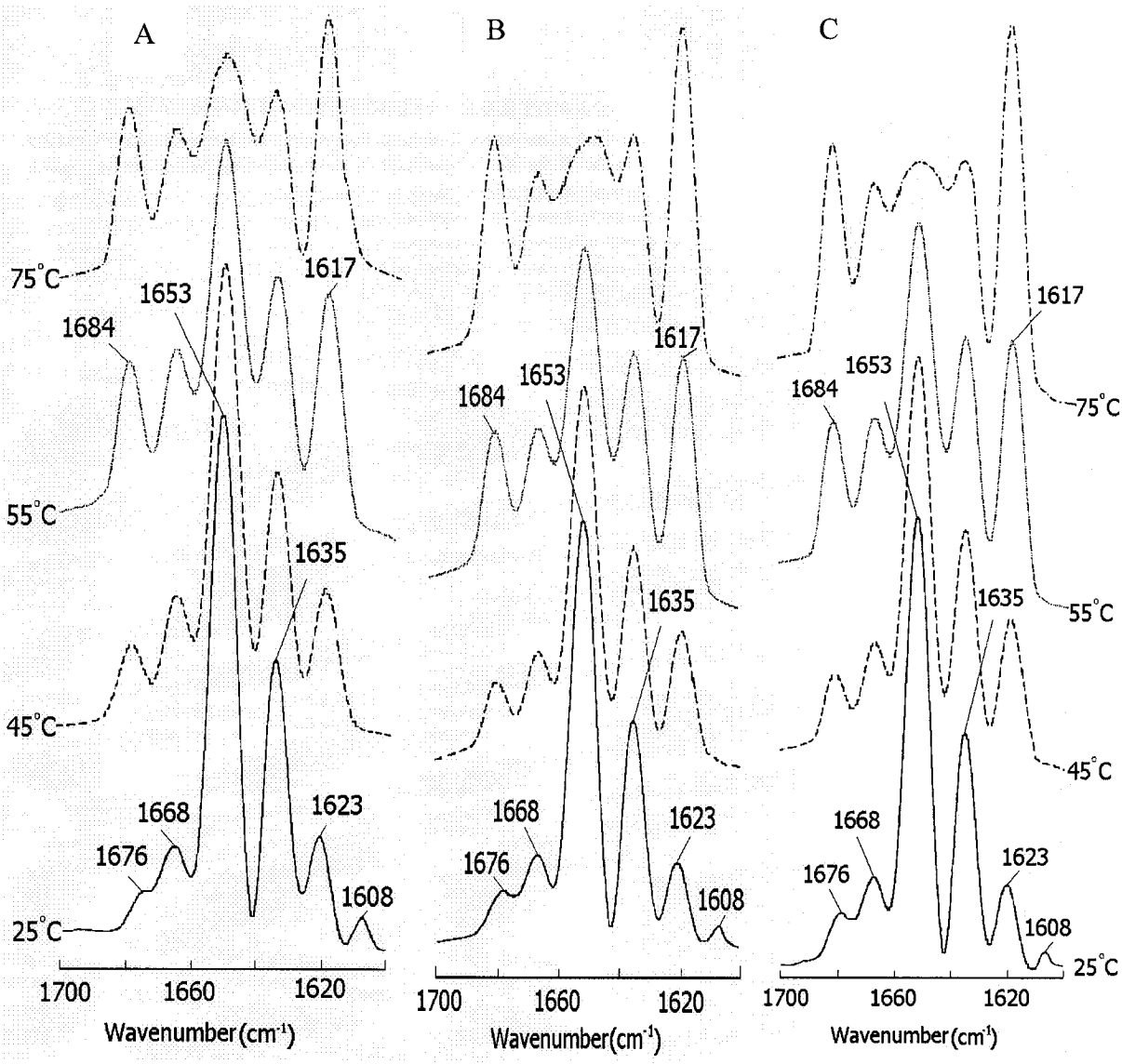

Fig 4.2: FTIR spectra of 3 mM deoxyHbA (A), deoxyHbA plus 2x BPG (B), and deoxyHbA plus 2x IHP (C) in 0.2 M NaPi buffer (pD 7.4) in the amide I′ (D_2O) region *vs* temperature. The experimental conditions are given in the legend of Figure 4.1. Contributions from BPG and IHP were subtracted from the spectra.

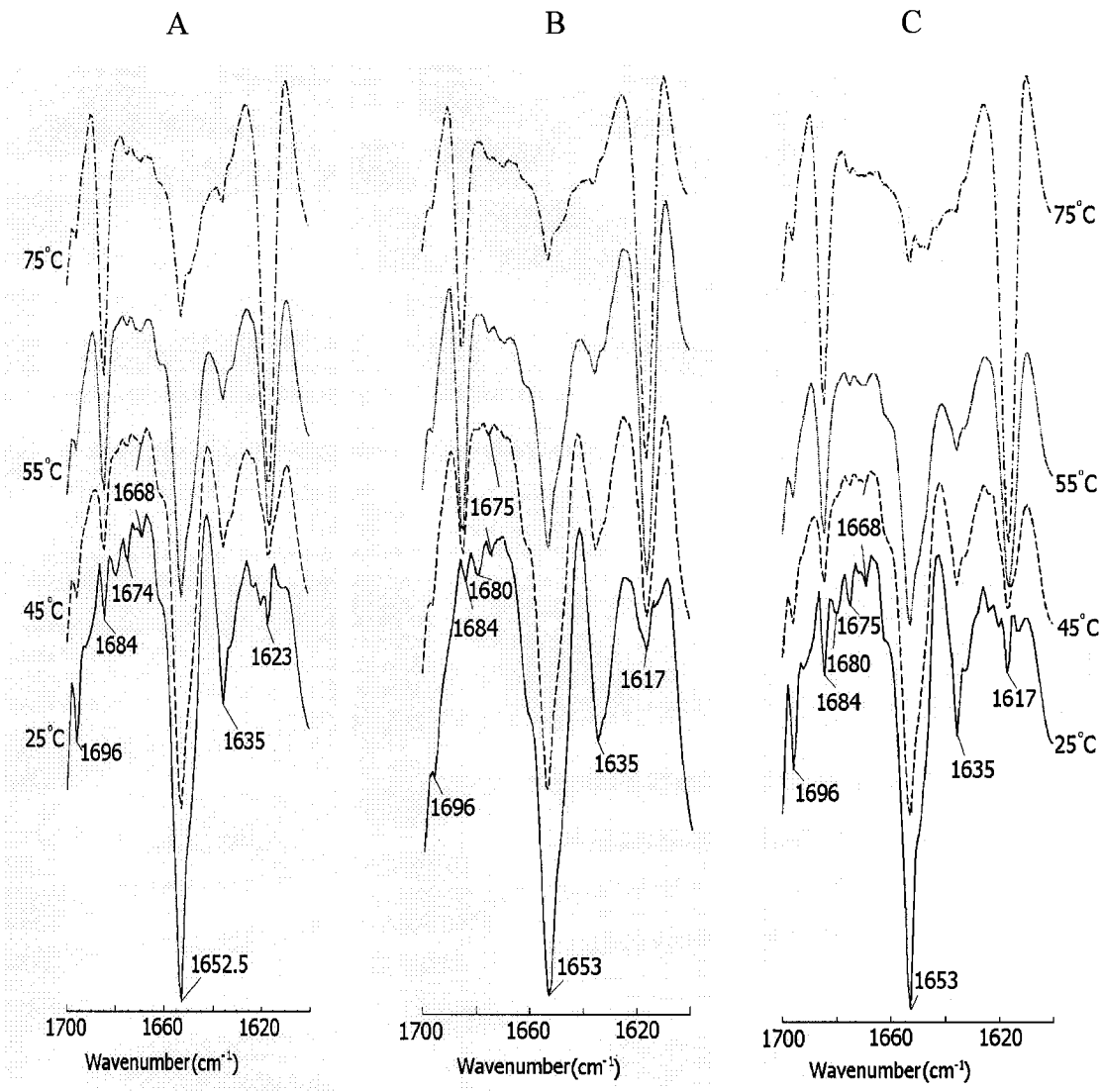

Fig 4.3: The second derivative FTIR spectra of 3 mM deoxyHbA (A), deoxyHbA plus 2x BPG (B), and deoxyHbA plus 2x IHP (C) in 0.2 M NaPi buffer (pD 7.4) in the amide I′ (D_2O) region *vs* temperature. The experimental conditions are given in the legend of Figure 4.2.

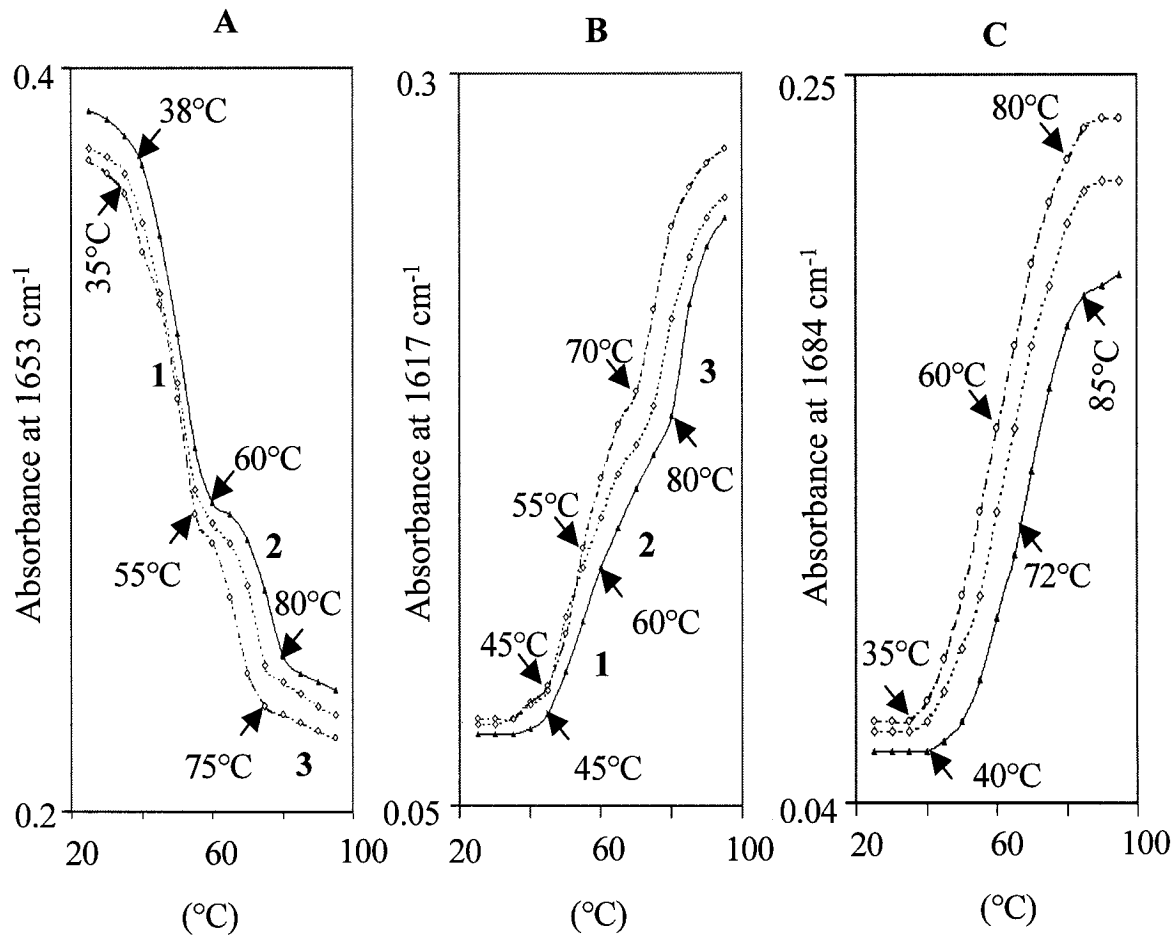

Fig 4.4: FTIR monitored thermal denaturation of deoxyHbA with and without effectors. Plots of absorbance at (A) 1653, (B) 1617 and (C) 1684 cm^{-1} of 3 mM deoxyHbA (triangles, solid line), deoxyHbA plus 2x BPG (diamonds, dashed line) and deoxyHbA plus 2x IHP (circles, dotted-dashed line) in 0.2 M NaPi buffer (pD 7.4) *vs* temperature. The α-helices are assumed to absorb at 1653 cm^{-1} and the aggregation bands at 1617 cm^{-1} and at 1684 cm^{-1}. The intensities were obtained from the spectra shown in Figure 4.2.

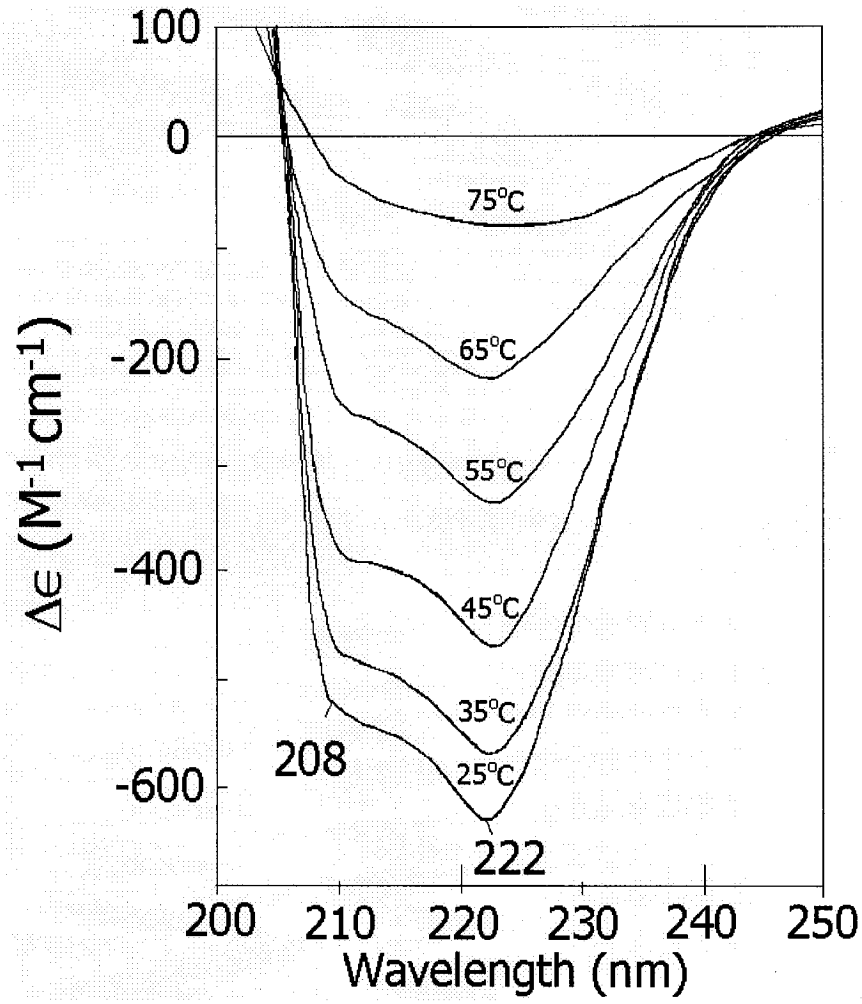

Fig 4.5: The far-UV CD spectra of 0.5 mM deoxyHbA in 0.2 M NaPi buffer (pH 7.4) *vs* temperature. The spectra were recorded at a HT reading <500 in the FTIR cell with a 50-μm pathlength. At each temperature the cell was equilibrated for 10 min and each spectrum is an average of 10 scans with a scan speed of 20 nm/min, a response time of 2 s and a slit of 0.2 nm. Buffer contributions were subtracted from each spectrum.

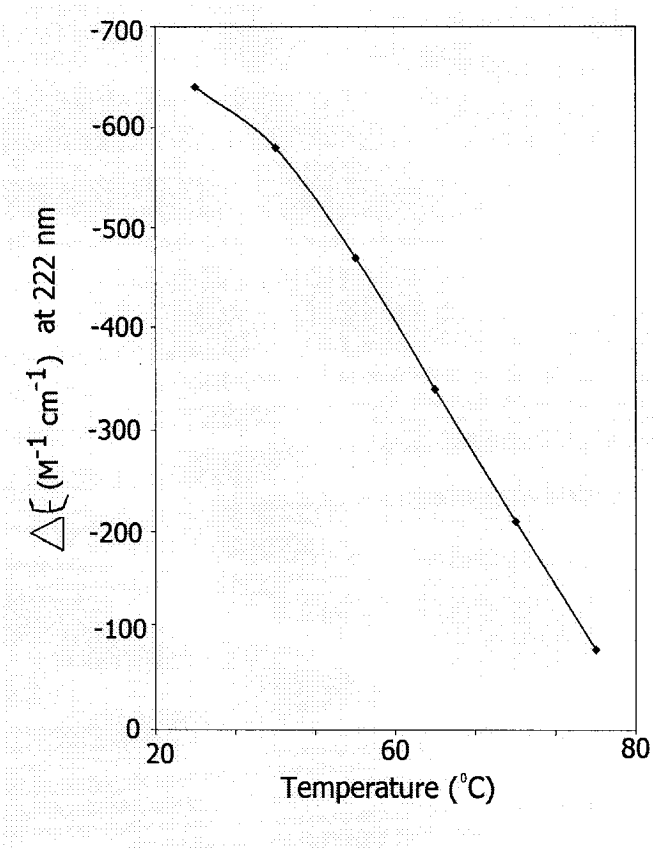

Fig 4.6: Plot of helical ellipticity at 222 nm of 0.5 mM deoxyHbA in 0.2 M NaPi buffer (pH 7.4) vs temperature. The Δε values were obtained from the spectra in Figure 4.5.

approximately 80% α-helical with turns connecting the helical segments but β-Structures are completely absent (44, 49). Susi and Byler deconvolved the amide I′ band of bovine metHb into three components at 1652 cm^{-1} for α-helical segments, and 1638 and 1675 cm^{-1} for turns (44). These authors also observed a band at 1623 cm^{-1} in β-lactoglobulin and suggested that this signal may be associated with a special kind of β-structure (44). Sire *et al.* studied the amide I′ spectra of oxyHb and carbonmonoxyHb at 20°C and observed four major components at 1672, 1654, 1635 and 1615-1619 cm^{-1} and assigned these to β-turns, α-helices, loops connecting the helical cylinders and subunit interactions in non-aggregated molecules, respectively (48). Schlereth and Mantele studied redox-induced conformational changes in myoglobin (Mb) and Hb by FTIR difference spectroscopy at surface-modified gold electrodes in an ultra-thin-layer spectroelectrochemical cell. They observed a large number of bands in the difference spectra between 1800-1000 cm^{-1} (50) that were assigned to the absorption of residues surrounding the heme and to the heme ring itself.

van Stokkum and his colleagues extensively studied the temperature induced conformational changes of several proteins (albumin, immunoglobin G, fibrinogen, lysozyme, α-lactalbumin and ribonuclease S) in D_2O and assigned the bands to different secondary structures (46). They observed a total of eight bands in the amide I/I′ region between 1700-1600 cm^{-1}. A minor band observed between 1600 and 1614 cm^{-1} is attributed to side-chain vibrations. At high temperature a band observed between 1616 and 1620 cm^{-1} is assigned to intermolecular β-sheet formation upon aggregation. Intramolecular β-sheet absorption is observed between 1632 and 1639 cm^{-1}. The random coil band is positioned between 1640 and 1650 cm^{-1}, and α-helical absorptions are

observed between 1651 and 1655 cm^{-1}. β-turns are observed between 1662 cm^{-1} and 1675 cm^{-1}, and the high energy absorption of antiparallel β-sheets occurs between 1680 and 1688 cm^{-1}.

In this study, a total of six bands (1608, 1623, 1635, 1653, 1668 and 1675 cm^{-1}) were observed in the amide I′ spectrum of deoxyHbA at 25°C in the presence and absence of BPG and IHP (Figures 4.1-4.3). The strong band at 1653 cm^{-1} that disappeared at higher temperatures is assigned to α-helical absorption, which accounts for ~80% of the secondary structure of Hb. A moderately strong band located at 1635 cm^{-1}, which also disappeared with increasing temperatures, is assigned to the nonhelical loops connecting the different helical segments. A band of medium intensity located at 1623 cm^{-1} is assigned to unordered structures. Weak bands at 1668 and 1675 cm^{-1} are assigned to β-turns. The two prominent bands that appear at 1684 and 1617 cm^{-1} at higher temperatures are assigned to aggregation bands (48).

A careful examination of the deconvolved and second derivative spectra (Figures 4.1-4.3) reveals complete loss of α-helical absorption at 75°C in effector-free deoxyHbA, while this takes place in the presence of BPG and IHP at 70 and 65°C, respectively. This suggests a destabilizing effect of these effectors on the secondary structures of deoxyHb. The plots of intensity at 1653 cm^{-1} *vs* temperatures appear to be triphasic (Figure 4.4A). The three phases extend over the temperature ranges 38-60, 60-80 and above 80°C in the absence of the effectors. These phases appear at ~5°C lower temperature in the presence of the effectors reflecting their destabilizing effects on the secondary structures of deoxyHbA. The plots of intensity *vs* temperature at 1617 cm^{-1} are also triphasic (Figure 4.4B). This confirms the triphasic loss of secondary structures. These phases appear at 5-

7 and 7-18°C lower temperature in BPG-deoxyHbA and IHP-deoxyHbA, respectively. Plots of the aggregation band at 1684 cm^{-1} are monophasic over 40-85°C with a Tm (midpoint temperature) of ~70°C in effector-free deoxyHbA and 65 and 60°C in BPG-deoxyHbA and IHP-deoxyHbA, respectively (Figure 4.4C), confirming the destabilizing effects of the effectors on the secondary structures of deoxyHbA.

The far-UV CD of deoxyHbA at 25°C exhibits the two negative peaks for α-helices at 208 and 222 nm with ellipticities of -530 and -640 $M^{-1}cm^{-1}$, respectively. With the rise in temperature, the absorption at these wavelengths decreases reflecting the loss of α-helical structure on heating. The plot of α-helical intensity at 222 nm *vs* temperature (Figure 4.6) resembles that of the FTIR aggregation band at 1684 cm^{-1} (Figure 4.4C) rather than that of the FTIR α-helical intensity (Figure 4.4A). This may be due to overlapping contributions of random structures to α-helical absorption. Also the different deoxyHbA concentrations used in the CD (0.5 mM) and the FTIR (3.0 mM) experiments may affect the thermal denaturation profiles. The far-UV CD spectra of effector-bound deoxyHbA were not recorded since the spectrum of effector-free deoxyHbA confirmed the FTIR results that loss of α-helical structures occurs on heating deoxyHbA.

Drzazga *et al.* studied the thermal stability of bovine metHb in both H_2O and 0.9% NaCl by differential scanning calorimetry (DSC). They also observed triphasic loss of secondary structures between 40 and 80°C (51), and suggested that the phases reflected tetramer to dimer dissociation, dimer to monomer dissociation and unfolding of monomers.

While the triphasic loss of secondary structures agrees with the DSC profile of bovine metHb denaturation (51), the destabilizing effects of the effectors on the

secondary structure of human deoxyHbA were unexpected. The spectroscopic data given in Chapters 3 and 4 suggest that BPG and IHP stabilize the $\alpha_1\beta_2$ interfaces of deoxyHbA. However, the loss of α-helical absorption and the appearance of aggregation bands at lower temperatures in effector-bound *vs* effector-free deoxyHbA (~55 *vs* 60°C) (Figure 4.4) indicate that the effectors destabilize regions of the protein at higher temperatures. In addition, broadening of Cysα104 ν(SH) absorption (Figures 2.1 and 2.2) below 55°C indicates that the effectors perturbed the $\alpha_1\beta_1$ interface even at 25°C. Thus, effector binding stabilizes the $\alpha_1\beta_2$ interface at the expanse of the $\alpha_1\beta_1$ interface, which is reflected in destabilization of secondary structures and lower aggregation temperatures.

5.0 Conclusions and Suggestions for Future Work

5.1 Conclusions

BPG and IHP stabilize the polar environment of Cysβ93 at the $\alpha_1\beta_2$ interface of deoxyHbA probably by stabilizing the salt bridges between the C-termini of the subunits. BPG and IHP also stabilize the heme pocket and the environment of aromatic residues (Tyrα42, Tyrα140, Trpβ37 and Tyrα145) at the $\alpha_1\beta_2$ interface.

The effectors destabilize the hydrophobic environment of Cysα104 and Cysβ112 at the $\alpha_1\beta_1$ interface. This may result from destabilizing or breaking the H-bonds between Cysα104 and Leuα100, or Cysβ112 and Asnβ108 or Valβ109.

The triphasic loss of α-helices suggests that the denaturation of secondary structures in deoxyHbA occurs in three phases both in the presence and absence of the effectors. The different plots shift by ~5-15°C to lower temperatures in effector-bound deoxyHbA indicating that these ligands destabilize the secondary structure of deoxyHbA. The three phases in the thermal denaturation are probably associated with the tetramer → $\alpha_1\beta_2$-dimer, $\alpha_1\beta_2$-dimer → monomer, and monomer → denatured monomer transitions. If the effectors destabilize the $\alpha_1\beta_1$ and $\alpha_2\beta_2$ interfaces, the tetramer→ $\alpha_1\beta_2$-dimer transition, which involves cleavages at these interfaces, should occur at lower temperatures in their presence. This would explain the shift in the thermal denaturation curves to the left (*i.e.,* lower temperature) seen in Figure 4.4.

5.2 Suggestions for Future Work

(1) Seven aromatic residues (Hisα58, Pheα33, Pheα43, Pheα98, Tyrα42, Tyrα140 and Trpα14) in the α-chain and nine (Hisβ63, Hisβ69, Pheβ41, Pheβ42, Pheβ71, Pheβ85, Pheβ103, Tyrβ130 and Trpβ15) in the β-chain are suggested to contribute to the heme cotton effect of HbA (29, 32, 38). The precise contributions of these residues have not been characterized. Ultraviolet resonance Raman (UVRR) spectroscopy can directly probe the environment of aromatic residues (53). Therefore, UVRR spectroscopy can be employed to determine the effects of BPG and IHP on the environments of the aromatic residues that contribute to the stabilization of the asymmetric heme environment of deoxyHbA.

(2) Drzazga *et al.* suggested that the triphasic loss of the secondary structures of bovine metHb on heating involves the dissociation of tetramer to dimer, dimer to monomer and finally unfolding of monomer (51). Convincing evidence to support this hypothesis has not been published so far. The sedimentation coefficients of Hb monomers, dimers and tetramer are different from one another (36). Thus, the measurement of sedimentation coefficients by analytical ultracetrifugation (AUC) at different temperatures should unveil the mechanism of the triphasic thermal denaturation of deoxyHbA.

(3) Bovine Hb has only one type of cysteine residue, Cysβ93, and equine and porcine Hbs possess Cysβ93 and Cysα104 but not Cysβ112 (19). FTIR investigations of the thermal stability of the ν(SH) absorption of these Hbs in the presence and absence of BPG and IHP would allow the effects of effector binding on the environment of Cysα104 to be examined in the absence of overlapping Cysβ112 absorption.

(4) The effects of BPG and IHP on the local and global conformational stabilities of metHb and oxyHb should be examined. Of particular interest are the effects of BPG on the ν(SH) vibrations of oxyHb given the critical role proposed for Cysβ93 in NO transport and delivery in red blood cells.

(5) A complete analysis of the far-UV CD spectra of deoxyHbA at higher concentration (3.0 mM) with and without the effectors present would complement the FTIR-monitored thermal denaturation profiles presented here using 3 mM protein. Similar analysis of the met and oxy forms of HbA should also be performed.

References

1. Perutz, M. F., Wilkinson A. J., Paoli, M. and Dodson, G. G. The Stereochemical Mechanism of the Cooperative Effects in Hemoglobin Revisited. Annu. Rev. Biophys. Biomol. Struct. (1998) 27, 1-34.

2. Perutz, M. F., Fermi G., Luisi, B., Shaanan, B. and Liddington, R. C. Stereochemistry of Cooperative Mechanisms in Hemoglobin. Acc. Chem. Res. (1987) 20, 309-321.

3. Perutz, M. F., Lander; J. E., Simon, S. R and Ho, C. Influence of Globin Structure on the State of the Heme. I. Human Deoxyhemoglobin. Biochemistry (1974) 13, 2163-2173.

4. Perutz, M. F., Fersht, A. R., Simon, S. R. and Robert, G. C. K. Influence of Globin Structure on the State of the Heme. II. Allosteric Transitions in Methemoglobin. Biochemistry (1974) 13, 2174-2186.

5. Perutz, M. F., Heidner, J. E., Lander, J. E., Beetlestone, J. G. S and Ho, C. Influence of Globin Structure on the State of the Heme. III. Changes in Heme Spectra Accompanying Allosteric Transitions in Methemoglobin and Their Implications for Heme-Heme Interactions. Biochemistry (1974) 13, 2187-2200.

6. Perutz, M. F., Kilmartin, J. V., Nagai K., Szabo, A. and Simon, S. R. Influence of Globin Structure on the State of the Heme. Ferrous Low Spin Derivatives. Biochemistry (1976) 15, 378-387.

7. Romeo, A. A., Capobianco, J. A. and English, A. M. Heme Nitrosylation of Deoxyhemoglobin by S-nitrosoglutathion Requires Copper. J. Biol. Chem. (2002) 277, 24135-241412.

8. Cheng, Y., Shen, T. J., Simplacea, V. and Ho, C. Ligand Binding Properties and Structural Studies of Recombinant and Chemically Modified Hemoglobins Altered at β93Cysteine. Biochemistry (2002) 41, 11901-11913.

9. Monod, J., Changeux, J. P. and Jacob, F. Allosteric Proteins and Cellular Control Systems. J. Mol. Biol. (1963) 6, 306-329.

10. Monod, J., Wyman, J., Changeux, J. P. On The Nature of Allosteric Transitions: A Plausible Model. J. Mol. Biol. (1965), 12, 88-118.

11. Khosland, D. E., Nemethy, G. and Filmer, D. Comparison of Experimental Binding Data and Theoretical Models in Proteins Containing Subunits. Biochemistry (1966) 5, 365-385.

12. Gelin, B. R., Lee, A. W. and Karplus, M. Hemoglobin Tertiary Structural Change on Ligand Binding. Its Role in the Co-operative Mechanism. J. Mol. Biol. (1983) 171, 489-559.

13. Nadolny, C., Kemf, I. and Zundel, G. Specific Interactions of the Allosteric Effector 2,3-Bisphosphoglycerate with Human Hemoglobin – A Difference FTIR Study. Biol. Chem. Hoppe-Seyler (1993) 374, 403-407.

14. Arnone, A. and Perutz M. F. Structure of Inositol Hexaphosphate-Human Deoxyhemoglobin Complex. Nature (1974), 249 (452) 34-36.

15. Kemp, I. and Zundel, G. The Allosteric Effector Molecule 2,3-Bisphosphoglycerate as A function of Protonation in Aqueous Solutions - An FTIR study. J. Mol. Strut. (1992) 269, 65-74.

16. Christiansen, J., Doughlas C. G., Halden, J. S. The Absorption and Dissociation of Carbondioxide by Human Blood. J. Physiol. (1914), 48, 244-277.

17. Van Beek, G. G. and De Bruin, S. H. Identification of the Residues Involved in the Oxygen-linked Chloride-ion Binding Sites in Human Deoxyhemoglobin and Oxyhemoglobin. Eur. J. Biochem. (1980) 105, 353-360.

18. Prange, H. D., Shoemaker, J. L., Westen, E. A., Horstkottle, D. G. and Pinshow, B. Physiological Consequences of Oxygen Dependent Chloride Binding to Hemoglobin. J. Appl. Physiol. (2001) 91, 33-38.

19. Bare, G. H., Alben, J. O. and Bromberg, P. A. Sulfhydryl Groups in Hemoglobin. A New Molecular Probe at the $\alpha_1\beta_1$ Interface Studied by Fourier Transform Infrared Spectroscopy. Biochemistry (1975) 14, 1578-1583.

20. Sampath, V., Zhao, X. J. and Caughey, W. S. Characterization of Interactions of Nitric Oxide with Human Hemoglobin A by Infrared Spectroscopy. Biochem. Biophys. Res. Commun. (1994) 198, 281-287.

21. Kandori, H., Kinoshita, N., Shichida, Y., Maeda, A., Needleman, R. and Lanyi, J. K. Cysteine S-H as a Hydrogen-Bonding Probe in Proteins. J. Am. Chem. Soc. (1998) 120, 5828-5829.

22. Dong, A. and Caughey, W. S. Infrared Methods for Study of Hemoglobin Reactions and Structures. Methods Enzymol. (1994) 232, 157-162

23. Guarrera, L., Colotti, G., Chiancone, E and Boffi, A. Ligand-linked Changes at the Subunit Interfaces in Scapharca Hemoglobins Probed Through the Sulfhydryl Infrared Absorption. Biochemistry (1999) 38, 10079-10083.

24. Boffi, A., Sarti, P., Amiconi, G. and Chiancone, E. The Interplay between Heme Iron and Protein Sulfhydryls in the Reaction of Dimeric Scapharca Inaequivalvis Hemoglobin with Nitric Oxide. Biophys. Chem. (2002) 98, 209-216.

25. Biochemicals and Reagents for Life Science Research. Sigma-Aldrich (2002-2003), Cat # D3258, 699.

26. Perutz, M. F., Muirhead, H., Cox, J. M. and Goaman, L. C. G. Three-dimensional Fourier Synthesis of Horse Oxyhemoglobin at 2.8 Å Resolution: The Atomic Model. Nature (1968) 219, 131-139.

27. Nagai, M., Sugita, Y. and Yoneyama, Y. Oxygen Equilibrium and Circular Dichroism of Hemoglobin- Rainier ($\alpha_2\beta_2$ $^{145\rightarrow Cys}$). J. Biol. Chem. (1972) 247, 285-290.

28. Guidotti, G. Studies on the Chemistry of Hemoglobin. J. Biol. Chem. (1967) 242, 3685-3693.

29. Geraci, G. and Parkhurst. L. J. Circular Dichroism Spectra of Hemoglobins. Method. Enzymology (1976), 76, 262-275.

30. Li, R., Nagai, Y. and Nagai, M. Contribution of α140Tyr and β37Trp to the Near-UV CD Spectra on Quaternary Structure Transition of Human Hemoglobin A. Chirality (2000) 12, 216-220.

31. Li, R., Nagai, Y. and Nagai, M. Changes of Tyrosine and Tryptophan Residues in Human Hemoglobin by Oxygen Binding: Near- and Far-UV Circular Dichroism of Isolated Chains and Recombined Hemoglobin. J. Inorg. Biochem. (2000) 82, 93-101.

32. Wajcman, H., Kister, J., Marden, M., Lahary, A., Monconduit, M. and Galacteros, F. Hemoglobin Rouen (α-140 (HC2) Tyr→His): Alteration of the α-Chain C-terminal Region and Moderate Increase in Oxygen Affinity. Biochim. Biophys. Acta (1992) 1180, 53-57.

33. Baldwin, J., and Chothiac, C. Hemoglobin: The Structural Changes Related to Ligand Binding and its allosteric Mechanism. J. Mol. Biol. (1979), 129, 175-220.

34. Sugita, Y., Nagai, M. and Yoneyama, Y. Circular Dichroism of Hemoglobin in Relation to the Structure Surrounding the Heme. J. Biol. Chem. (1971) 246, 383-388.

35. Nagai, M., Sugita, Y. and Yeneyama, Y. Circular Dichroism of Hemoglobin and Its Subunits in the Soret Region. J. Biol. Chem. (1969) 244, 1651-1653.

36. Craik, C. S., Vallette, I., Beychok, S. and Walks, M. Refolding Defects in Hemoglobin Rothschild. J. Biol. Chem. (1980) 255, 6219-6223.

37. Kleckner, H. B., Wilson, J. B., Lindeman, J. G., Stevens, P. D., Niazi, G., Hunter, E., Chen, C. J. and Huisman, T. H. Hemoglobin Fort Gordon or $\alpha_2\beta_2$ $^{145\ Tyr\rightarrow Asp}$, A New High-Oxygen Affinity Hemoglobin Variant. J. Biochim. Biophys. Acta (1975) 400, 341-347.

38. Hsu, H. C. and Woody, R. W. The Origin of Heme Cotton Effects in Myoglobin and Hemoglobin. J. Am. Chem. Soc. (1971), 93, 3515-3525.

39. Shaanan, B. Structure of Human Oxyhemoglobin at 2.1 Å Resolution. J. Mol. Biol. (1983) 171, 31-59.

40. Strictland, E. H., Wilchek, M., Horwitz, J. and Billups, C. Effects of Hydrogen Bonding and Temperature Upon the Near Ultraviolet Circular Dichroism and Absorption Spectra of Tyrosine and O-Methyl Tyrosine Derivatives. J. Biol. Chem. (1972) 247, 572-580.

41. Matsukawa, S., Nishibu, M., Mawatari, K. and Yoneyama, Y. Analysis of Optical Properties of Hemoglobins in Terms of the Two-state Model, Especially from Studies of the Abnormal Hemoglobins with Amino Acid substitution in the $\alpha_1\beta_2$ Contact Region. J. Biol. Chem. (1979) 232, 247-266.

42. Geraci, G. and Sada, A. Reactivity of the 93 Sulfhydryls of Human Haemoglobin A: Influence of the C-Terminal Residues. J. Mol. Biol. (1972) 70, 729-734.

43. Liem, R. K. H., Calhoun, D. B., Englander, J. J. and Englander, S. W. A High Energy Structure Change in Hemoglobin Studied by Difference Hydrogen Exchange. J. Biol. Chem. (1980), 1087-1094.

44. Susi, H. and Byler, D. M. Protein Structure by Fourier Transform Infrared Spectroscopy: Second Derivative Spectra. Biochem. Biophys. Res. Commun. (1983) 115, 391-397.

45. Filosa, A. and English, A. M. FTIR Monitored Thermal Titration Reveals Different Mechanisms for the Alkaline Isomerization of Tuna Compared to Horse and Bovine Cytochromes C. J. Biol. Inorg. Chem. (1999) 4, 717-726.

46. Van Stokkum, I. H. M., Linsdell, H., Hadden, J. M., Haris, P. I., Chapman, D. and Blomendal, M. B. Temperature-Induced Changes in Protein Structures Studied by Fourier Transform Infrared Spectroscopy and Global Analysis. Biochemistry (1995) 34, 10508-10518.

47. Ruckebush, C., Nedjar-Arroume, N., Magazzeni, S., Huvenne, J. P. and Legrand, P. Hydrolysis of Hemoglobin Surveyed by Infrared Spectroscopy: I. Solvent Effect on the Secondary Tructure of Hemoglobin. J. Mol. Struct. (1999) 478, 185-191.

48. Sire, O., Zentz, C., Pin, Serge, Chinsky, L.,Turpin, P. Y., Martel, P., Wong, P. T. T. and Alpert, B. Long-Range Effects in Liganded Hemoglobin Investigated by Neutron and UV Raman Scattering, FTIR and CD spectroscopies. J. Am. Chem. Soc. (1997) 119, 12095-12099.

49. Levitt, M. and Greer, J. Automatic Identification of Secondary Structure in Globular Proteins. J. Mol. Biol, (1977) 114, 181-239.

50. Schlereth, D. D. and Mantele, W. Redox Induced Changes in Myoglobin and Haemoglobin: Electrochemistry and Ultraviolet-Visible and Fourier Transform Infrared Difference Spectroscopy at Surface Modified Gold Electrodes in an Ultra-Thin Layer Spectroelectrochemical Cell. Biochemistry (1992) 31, 7494-7502.

51. Drzazga, Z., Michnik, A., Bartoszek, M. and Beck, E. Thermal Stability of Hemoglobin Solutions Under DC and AC Magnetic Fields and UV and IR Radiation. J. Tharm. Ana. Cal. (2001) 65, 575-582.

52. Kristinsson, H. G. Acid-Induced Unfolding of Flounder Hemoglobin: Evidence for a Molten Globular State with Enhanced Pro-oxidative Activity. J. Agric. Food Chem. (2002) 50, 7669-7676.

53. Su, C., Park, Y.D, Liu, G. Y, and Spiro, T. G. Hemoglobin Quaternary Structure Change Monitored Directly by Transient UV Resonance Raman Spectroscopy. J. Am. Chem. Soc. (1989) 111, 3457-3459.